Transformers Don't Need LayerNorm at Inference Time: Scaling LayerNorm Removal to GPT-2 XL and the Implications for Mechanistic Interpretability

Anonymous Author(s)
Affiliation
Address
email

Abstract

Layer-wise normalization (LN) is an essential component of virtually all transformer-based large language models. While its effects on training stability are well documented, its role at inference time is poorly understood. Additionally, LN layers hinder mechanistic interpretability by introducing additional nonlinearities and increasing the interconnectedness of individual model components. Here, we show that all LN layers can be removed via fine-tuning from every GPT-2 model with only a small increase in validation loss (e.g. +0.03 cross-entropy loss for GPT-2 XL). Thus, LN is not essential at inference to maintain comparable performance in language modeling. We find that the amount of fine-tuning data needed for LN removal grows sublinearly with model parameters, suggesting scaling to larger models is feasible. We release a suite of LN-free GPT-2 models on Hugging Face. Furthermore, we test interpretability techniques on LN-free models. Direct logit attribution now gives the exact direct effect of individual components, while the accuracy of attribution patching does not significantly improve. We also confirm that GPT-2's "confidence neurons" are inactive in the LN-free models. Our work clarifies the role of LN layers in language modeling, showing that GPT-2-class models can function without LN layers. We hope that our LN-free analogs of the GPT-2 family of models will enable more precise interpretability research and improve our understanding of language models.

1 Introduction

Large language models (LLMs) have seen widespread adoption in recent years [Touvron et al., 2023, OpenAI et al., 2024, Gemini Team et al., 2024], most of which are based on the Transformer architecture Vaswani et al. [2017]. A key component of virtually all such LLMs are layer-wise normalization (LN) layers, typically LayerNorm [Ba et al., 2016]

$$\mathrm{LN}(\mathbf{x}) = \frac{\mathbf{x}-\mu}{\sigma} \odot \boldsymbol{\gamma} + \boldsymbol{\beta}, \quad \mu = \frac{1}{H}\sum_{h=1}^{H} x_h, \quad \sigma = \sqrt{\frac{1}{H}\sum_{h=1}^{H}(x_h-\mu)^2 + \epsilon}, \tag{1}$$

or RMSNorm [Zhang and Sennrich, 2019, same formula without subtracting the mean μ]. These layers have been introduced to stabilize the training process [Ba et al., 2016], similar to batch normalization [Ioffe and Szegedy, 2015] in other network architectures.

Unlike batch normalization however, LN layers cannot be replaced with a linear transformation at inference time. While the mean centering (μ), weight ($\boldsymbol{\gamma}$), and bias ($\boldsymbol{\beta}$) parameters can be folded into neighboring layers [e.g. `fold_ln`, Nanda and Bloom, 2022], the non-linear division by the norm or

Submitted to 39th Conference on Neural Information Processing Systems (NeurIPS 2025). Do not distribute.

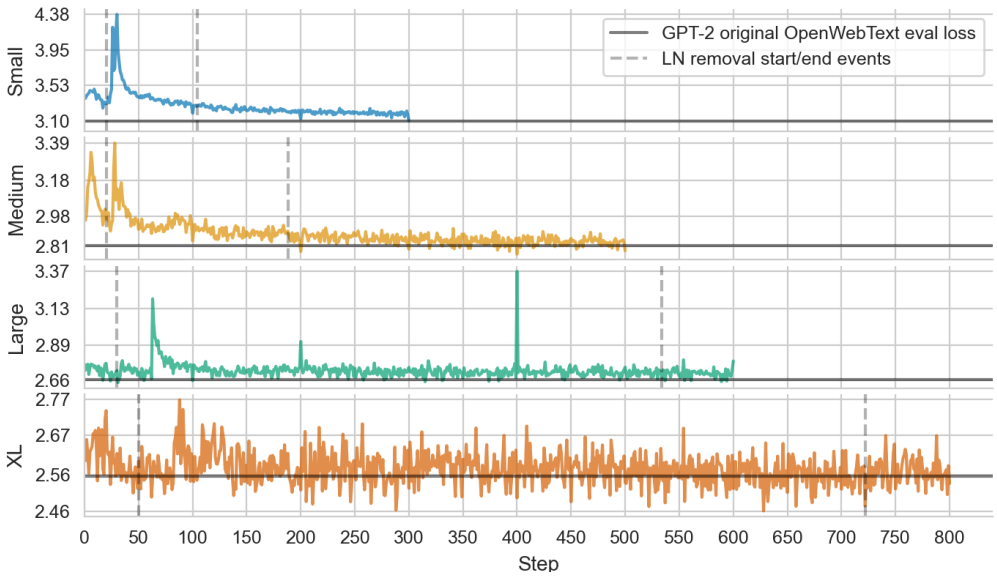

Figure 1: Main training loss curves for all GPT-2 variants during LN removal. Original GPT-2 OpenWebText eval losses are shown for reference. Curves terminate at model suite checkpoints. LN removal period shown as vertical lines.

standard deviation of the residual stream must be executed at inference time. This raises the question of what role LNs plays in the model and whether it is necessary for the model to function. Prior work has shown that LNs functions can implement complex non-linear functions in toy models [Winsor, 2022], and proposed that LNs might play a role in confidence regulation in LLMs [Stolfo et al., 2024].

Additionally, LN layers complicate mechanistic interpretability. Mechanistic interpretability typically aims to decompose the model into smaller components and to understand their individual effects and interactions. Both of these are complicated by the non-linearity of LN layers. Individual components cannot be easily attributed as their effect on LN depends on the residual stream activations ([nostalgebraist, 2020, Elhage et al., 2021, Wang et al., 2022b, Nanda, 2023b],Nanda [2023a]). Interactions between components are also complicated by LN because it causes each component to affect almost every downstream component in the model (via the LN scale). This makes analyzing the interactions complex [e.g. Bushnaq et al., 2024, Farnik et al., 2025]. In practice, researchers approximate the LN layers as linear transformations [referred to as "freezing LayerNorm"; Bricken et al., 2023, McDougall et al., 2023, Kissane et al., 2024], or train models without LN layers [Elhage et al., 2021, Nabeshima, 2024].

In this work we show that LN layers can be removed from transformer models at the end of training. We replace the LN layers with a linear transformation that is initialized to be close to the original LN transformation, and fine-tune the model on a small fraction of its training data. We do this for one LN layer at a time, essentially slowly weaning the model off of LN. This (a) shows that LLMs can function without LN layers, and (b) provides a LN-free versions of the GPT-2 family of models. These models can be studied on their own, simply to understand any large language model, or as a proxy for their corresponding original GPT-2 models. The latter is possible as our fine-tuned models have similar internals, but should be used with caution as similarity is not exact.

Our contribution is threefold:

- We show that LLMs can function without LN layers, achieving a cross-entropy loss comparable to the original models.
- We provide a optimized protocol for removing LN layers from LLMs at the end of training or during fine-tuning, and provide a suite of LN-free GPT-2 models on Hugging Face.

- We validate that the interpretability of LN-free models is improved, finding that the direct logit attribution (DLA) error is reduced from 50% to 0%, and that attribution patching—contrary to expectations in the literature—does not improve with LN-free models.

2 Related work

Mechanistic interpretability: Interpretability aims to understand the internals of neural networks and the algorithms they implement. Most mechanistic interpretability methods attempt to decompose a model into smaller components and aim to understand the interactions between those components. The most popular methods are based on sparse dictionary learning, such as sparse autoencoders [Bricken et al., 2023] or cross-layer transcoders [Ameisen et al., 2025]. In both cases, researchers attempt to find a sparsely-interacting set of components that explain the model's behavior [Marks et al., 2024, Lindsey et al., 2025]. The most common approach to deal with LN is to approximate the layer norm scale as constant [e.g. Bricken et al., 2023, McDougall et al., 2023, Kissane et al., 2024]. Other methods introduce special cases for LN layers [e.g. Bushnaq et al., 2024].

LN alternatives: The main alternative to layer normalization is batch normalization (BN). However, BN performs worse than LN in language model transformers due to changes between the training and inference distributions [e.g. Wang et al., 2022a].

Concurrent work [Zhu et al., 2025] proposed a Dynamic Tanh (DyT) as an alternative to normalization. Instead of an LN layer, they apply an element-wise $\tanh(\alpha x)$ function to the residual stream. This work confirms our results, finding that language models can work without LN. While DyT is preferable over LN, in some use cases, DyT is still a non-linear function whose role we don't understand, and that affects interpretability. Our work goes further, replacing LN with a purely linear transformation.

Transformers trained without normalization: Finally, Nabeshima [2024] trains toy language models from scratch, without normalization. However, we expect this method to work only for small language models, state-of-the-art language models continue being trained with normalization. Thus we focus on removing LN from an already-trained model.

3 LN Removal strategy and methods

We remove the nonlinearity of LN by replacing the standard deviation in (1) by a scalar, corresponding to an estimate of the average standard deviation, $\overline{\sigma}_{\text{avg}}$, while fine-tuning on OpenWebText. We define a FakeLN block as

$$\text{FakeLN}(\mathbf{x}) = \frac{\mathbf{x}-\mu}{\overline{\sigma}_{\text{avg}}} \odot \boldsymbol{\gamma} + \boldsymbol{\beta}, \quad \sigma_{b,s} = \sqrt{\frac{1}{H}\sum_{h=1}^{H}(x_{b,s,h}-\mu_{b,s})^2 + \epsilon}, \quad \sigma_{\text{avg}} = \frac{1}{BS}\sum_{b=1}^{B}\sum_{s=1}^{S}\sigma_{b,s}, \tag{2}$$

where $\sigma_{b,s}$ is the standard deviation across the model dimension for batch index b and sequence position s, and σ_{avg} is the average across all tokens in a batch. $\overline{\sigma}_{\text{avg}}$ is the fixed scalar value used when replacing LN with FakeLN. Because removing all LN blocks simultaneously irreparably breaks the model's performance, we adopt a sequential removal process during fine-tuning: we remove one LN block, fine-tune for a fixed number of steps to stabilize the loss (which typically spikes after each removal), and then proceed to the next LN block. Furthermore, σ_{avg} can drift during fine-tuning. Therefore, to minimize the disruption introduced by LN removal and stabilize the fine-tuning process, we recompute σ_{avg} for each batch and freeze the scaled factor in FakeLN at the moment of removal to $\overline{\sigma}_{\text{avg}} = \sigma_{\text{avg}}$. For the small and medium models, the batch size is significantly large enough to produce reliable estimates of σ_{avg}. For GPT-2 Large and GPT-2 XL, we use an exponential moving average filter to update σ_{avg} for new batches. After LN removal, $\overline{\sigma}_{\text{avg}}$ is not updated anymore.

We categorize LN blocks into LN^l_{qk}, LN^l_{v}, LN^l_{MLP} and LN^f, where l indicates the layer number. Respectively, these LN blocks normalize inputs to the query/key path, the value path, the MLP, and the final unembedding. While splitting LN for attention heads paths is uncommon, we find this more fine-grained removal of LN improves stability during fine-tuning. Our sequential removal process begins after an initial standard fine-tuning phase with the removal of LN^0_{MLP}, followed by g_{mlp}

fine-tuning steps. We then remove LN^1_{MLP}, fine-tune again for g_{mlp} steps and continue this pattern layer by layer until LN^L_{MLP} is removed where $L = N_{\text{layers}}$. We then apply the same pattern to remove LN^l_{qk} and LN^l_{v} blocks, each separated by g_{qk} and g_{v} fine-tuning steps, respectively. Finally, we remove LN^f. The gaps between removal events are hyperparameters that have to be chosen carefully. Too small gaps can result in instabilities, while choosing very large gaps results in unnecessarily high computational costs. We provide a table with LN removal schedule and more details in Appendix B.

We empirically found that beginning with LN^{MLP}_l rather than LN^{qk}_l led to more stable fine-tuning, likely because residual norm variance at beginning-of-sequence tokens affects the attention mechanism more strongly when its normalization is removed first. Despite removing LN blocks sequentially, instabilities can still occur during LN removal. To further stabilize LN-removal by fine-tuning, we used an additional auxiliary loss.

Auxiliary Loss In models with LN, residual stream vectors are scaled by their standard deviation[1]. When LN is removed, large norm disparities across positions can lead to gradient spikes and destabilize fine-tuning. To encourage stable activations during this process, we introduce an auxiliary loss that promotes consistent standard deviations across token positions:

$$\mathcal{L}_{\text{aux}} = \lambda \cdot \mathbb{E}_{b,s}\left[(\sigma_{b,s} - \hat{\sigma})^2\right], \qquad \hat{\sigma} = \frac{1}{|\mathcal{M}|}\sum_{(b,s)\in\mathcal{M}} \sigma_{b,s}, \tag{3}$$

where λ is a scalar hyperparameter. While the loss itself is computed across all positions in the batch, the target $\hat{\sigma}$ is the average standard deviation across the subset of token positions $\mathcal{M}$, excluding the first token (position 0) and any positions containing the end-of-text token (ID 50256). These exclusions from the target calculation are motivated by the observation that such positions consistently exhibit higher variance in GPT-2 models. We apply the auxiliary loss only at LN^f since all residual streams propagate through this final normalization layer, making it a natural global target for norm regularization.

4 LN Removal results

We successfully remove LN during fine-tuning on OpenWebText from GPT-2 Small, Medium, Large, and XL (Tab. 1), demonstrating that our sequential LN removal strategy with auxiliary loss scales from a 124 million parameter model to a 1.5 billion parameter model. Figure 1 shows the main loss during fine-tuning for LN-removal (for details of the sequential LN-removal schedule and hyperparameters, see Appendix B). We find that the largest main loss spikes appear during the removal of LN_{MLP} blocks, which is the first LN block that is removed. The LN_{qk} and LN_{v} block removals result only in small main loss spikes. Before introducing the auxiliary loss, the LN-removal fine-tuning loss curves were more spiky, suggesting that the auxiliary loss effectively absorbs some of the effects of LN removal. Furthermore, the auxiliary loss decreases quickly at the beginning of fine-tuning, indicating that the model successfully learns to maintain consistent standard deviations across token positions.

As a control, we compare the LN-free GPT-2 model suite to the original GPT-2 models and vanilla fine-tuned models. The vanilla fine-tuned models were fine-tuned for the same number of steps and with the same learning rate schedule as the LN-free models, but without auxiliary loss and without removing LN. This control allows us to disentangle the effects of LN from the effects of fine-tuning.

We evaluate performance using mean cross-entropy loss on a validation set of OpenWebText, The Pile, and The Pile-filtered (Tab. 1). The Pile-filtered consists of sequences from The Pile dataset (monology-pile-uncopyrighted), filtered by removing sequences containing tokens that appear in The Pile but not in OpenWebText, such as control characters which arise from formatting discrepancies between the two datasets (see Appendix D for more details).

We find that LN-free models perform comparably to their original variants, with performance gaps ranging from +0.03 to 0.1 cross-entropy loss difference on The Pile-filtered (Tab.,1). This comparable performance extends to standard language understanding benchmarks, where LN-free models maintain accuracy within 1-2 percentage points from their original variants (Appendix E).

[1] After subtracting the mean across features, i.e., removing the component in the $[1, 1, \ldots, 1]$ direction [Gupta et al., 2025].

Table 1: Overview of our LN-free, vanilla fine-tuned, and original GPT-2 models. Reported values are mean cross-entropy losses for 10.2M tokens for The Pile and The Pile filtered and 4.5M tokens for the OpenWebText (WT) validation set. For each model size and dataset, the lowest loss is highlighted in bold, and the loss difference between the LN-free model and the best-performing model is shown in brackets. All models are available on Hugging Face, see Appendix A. We also discuss compute requirements in Appendix A.

Model	FT steps	OWT (val)	The Pile	The Pile-filtered
GPT-2 Small original	0	3.1006	**2.8450**	**2.7899**
GPT-2 Small vanilla	300	**3.0126**	2.8511	2.8112
GPT-2 Small LN-free	300	3.0797 [+0.0671]	2.8852 [+0.0402]	2.8757 [+0.0858]
GPT-2 Medium original	0	2.8145	**2.5163**	**2.5390**
GPT-2 Medium vanilla	500	**2.7390**	2.5752	2.5724
GPT-2 Medium LN-free	500	2.7642 [+0.0252]	2.6579 [+0.1416]	2.6352 [+0.0962]
GPT-2 Large original	0	2.6623	**2.5320**	**2.4347**
GPT-2 Large vanilla	600	**2.6240**	2.6233	2.5074
GPT-2 Large LN-free	600	2.6384 [+0.0144]	2.7504 [+0.2184]	2.5159 [+0.0812]
GPT-2 XL original	0	2.5567	**2.4436** [2]	**2.3739**
GPT-2 XL Vanilla	800	**2.4799**	2.4673	2.3821
GPT-2 XL LN-free	800	2.5052 [+0.0253]	130.2197 [3]	2.3992 [+0.0253]

The only notable exception is GPT-2 XL LN-free, which shows degraded performance on The Pile. A closer examination of the distribution of losses reveals that the higher averaged CE loss is driven by a very small number of samples and that the 99.9 percentile ranges of GPT-2 XL LN-free and GPT-2 original are nearly identical for The Pile, indicating that the vast majority of sequences are handled similarly by both models. This suggests that GPT-2 XL LN-free is highly overconfident on a small number of sequences that are present in The Pile but absent from The Pile-filtered dataset.

We also investigate whether the performance gap can be closed by simply fine-tuning LN-free models for longer. Contrary to our initial expectations, we find that extending fine-tuning does not reduce the loss gap to vanilla models. Instead, the gap remains approximately constant throughout fine-tuning, suggesting that LN contributes a small but persistent performance benefit that cannot be compensated by additional fine-tuning. We discuss potential mechanisms behind this behavior in Section 5.4. We also investigate if our methodology generalizes beyond the GPT2 model family, and successful apply our removal strategy to Pythia 70M [Biderman et al., 2023] (see Appendix C).

5 Mechanistic interpretability analyses on LN-Free models

Removing LN eliminates nonlinear dependencies between components and results in models where residual stream directions map linearly to output logits. In this section, we evaluate common interpretability methods, such as Direct Logit Attribution (DLA) [nostalgebraist, 2020, Elhage et al., 2021, Wang et al., 2022b, Nanda, 2023b] and attribution patching [Nanda, 2023a] on LN-free models and compare the results to their counterparts with LN.

5.1 Direct Logit Attribution on LN-free models gives exact Direct Effect on logits

Direct Logit Attribution (DLA) is an approximation to the Direct Effect (DE) of a component. The DE [Pearl, 2022, Geiger et al., 2024] is the effect of a model component on the outputs that is not mediated by intermediate components, and can be computed by subtracting a component's output c from the residual stream r after the final layer, and taking the difference in outputs,

$$\mathrm{DE}(c) = \mathrm{LN}(r) \cdot W_U - \mathrm{LN}(r - c) \cdot W_U, \tag{4}$$

[2] GPT-2 XL original: Median: 1.0103, 95 Percentile range: [0.0005, 10.6193], 99.9 percentile range [≈0.0000, 43.0064]

[3] GPT-2 XL LN-free: Median: 1.0937, 95 percentile range: [0.0004, 10.7548], 99.9 percentile range [≈0.0000, 48.6459]

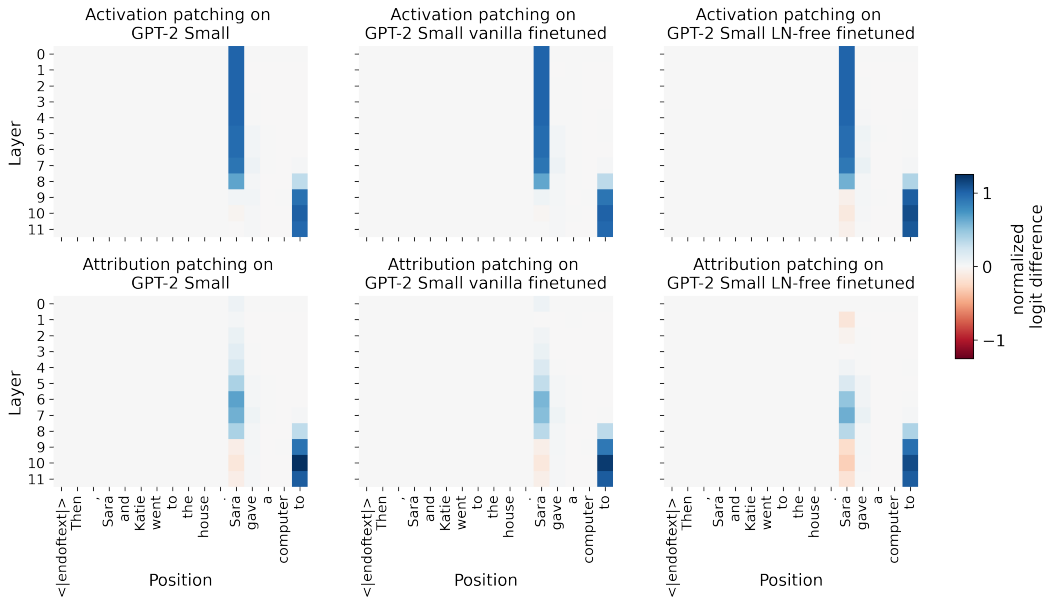

Figure 2: Activation patching and attribution patching applied on the residual stream at different layers and positions on GPT-2 Small and the corresponding vanilla and LN-free versions.

where W_U denotes the unembedding, and LN the final LayerNorm. The DLA approximation is computed using the cached LN scale,

$$\text{DLA}(c) = \text{LN}_{\text{cached}}(c) \cdot W_U, \tag{5}$$

which effectively linearizes LayerNorm (LN).

We calculated both DLA and DE on each attention head in GPT-2 Small original, GPT-2 Small vanilla FT, and GPT-2 Small LN-free FT, on 1,000 sequences of consisting of 512 tokens from The Pile-filtered, for logits corresponding to the correct target token. To compare metrics, we used the Normalized Mean Absolute Error (NMAE)[4], which measures the average discrepancy between DLA and DE, expressed as a percentage of the average magnitude of the DE. Our LN-free fine-tuned model achieves a perfect 0.00% [0.00%, 0.00%] (95% Confidence Interval - CI) NMAE, whereas the original model exhibits an NMAE of 49.07% [29.92%, 66.10%]. This result shows that removing LNs makes these methods mathematically equivalent, eliminating the need for inaccurate linearization approximations. See Appendix F for more details.

5.2 Accuracy of attribution patching on LN-free models does not significantly improve

Activation patching [Meng et al., 2022, Zhang and Nanda, 2023, Heimersheim and Nanda, 2024] is an interpretability method used to assess the causal roles of neural network components by transferring activations from a "clean" prompt that elicits correct model behavior into a "corrupted" prompt that typically leads to incorrect behavior. Formally, this can be expressed as:

$$\Delta = f(x_{\text{corr}}; a_l \leftarrow a_l(x_{\text{clean}})) - f(x_{\text{corr}}), \tag{6}$$

where $f(x)$ measures differences in model predictions (typically logit differences), and $a_l \leftarrow a_l(x_{\text{clean}})$ indicates replacing the corrupted activation with its clean counterpart at layer l. While precise, activation patching is computationally expensive, scaling with the number of components tested. Attribution patching Nanda [2023a] addresses this approximating activation patching with a first-order Taylor expansion around the corrupted activation, requiring only two forward passes and one backward pass,

$$\Delta = f(x_{\text{corr}}; a_l \leftarrow a_l(x_{\text{clean}})) - f(x_{\text{corr}}) \approx \nabla_{a_l} f(x_{\text{corr}}) \cdot (a_l(x_{\text{clean}}) - a_l(x_{\text{corr}})) = \Delta_{\text{attr}}. \tag{7}$$

[4]We calculate NMAE, using averages of absolute differences and DE magnitude rather than per-sample ratios, as we did not observe a consistent proportional relationship between these two measures across samples.

As LN projects residual vectors onto a $(d_{\text{model}} - 1)$-dimensional sphere after removing the mean component, it causes derivatives to vanish when patched directions align with the residual stream and is, therefore, a source of attribution patching errors, i.e. discrepancies between attribution patching estimates and ground-truth activation patching results (Neel Nanda described it for this reason as "*a particularly thorny nonlinearity*"[Nanda, 2023a]).

We investigate whether LN is the primary factor limiting attribution patching accuracy by compared attribution patching across three models: GPT-2 Small, the corresponding LN-free fine-tuned, and vanilla fine-tuned. We focused on the residual stream preceding each transformer block, a location where attribution patching is known to perform particularly poorly in models with LN. We used 480 IOI Wang et al. [2022b] prompts, systematically varying names, places, and objects, with each prompt paired with counterparts covering all possible name orderings. To ensure alignment across inputs, all prompts had fixed token lengths and name positions. We applied both techniques and quantified how well attribution patching approximates activation patching across layers. We used normalized logit differences as the patching metric to enable robust comparisons across methods. Surprisingly, attribution patching yielded very similar results across layers in the three models (see Fig. 2) and despite removing LN, we observed no improvement in attribution patching accuracy. For each layer, we quantified this by computing the sum of absolute attribution patching errors across token positions in the vanilla fine-tuned model, and subtracting the corresponding value from the LN-free model. This yielded a per-layer improvement score, where positive values indicate lower attribution error in the LN-free model. Averaged across layers, the improvement is $\mu = -0.026$, with standard deviation $\sigma = 0.082$. This negative but informative result suggests that attribution patching's limitations likely arise from other more fundamental nonlinearities in the transformer architecture, namely the attention SoftMax or the MLP activation functions.

5.3 First position tokens are no longer special

A well-documented phenomena in transformer-based language models is the disproportionately high L2 norm of first position token's hidden representations [Xiao et al., 2024, Yona et al., 2025, Barbero et al., 2025]. This characteristic has been identified as a key mechanism behind "attention sinks," where the first token captures an outsized portion of attention across multiple heads, affecting information flow throughout the network. While this mechanism appears to help standard models avoid representational collapse by controlling information mixing across layers, it introduces computational irregularities and potential vulnerabilities [Yona et al., 2025].

To investigate whether our models exhibit similar behaviours, we measured the L2 norm of first position tokens, compared to all other tokens, on 1,000 sequences consisting of up to 512 tokens from The Pile-filtered. LN-free models reveal a disruption of the typical first position token norm pattern. As illustrated in Fig. 3, the LN-free model maintains consistently moderate L2 norm values ($\sim$300 to 500) across all layers for the first token, in contrast to the significant norm inflation observed in models with LN. This more uniform norm across token positions represents a fundamental shift from the standard architecture, where the first token's norm typically exceeds that of other tokens by close to an order of magnitude. The largest first token norm growth in all three models was due to the attention head in layer 3, where norms grow from $\sim$500 to 3,600 for the models with LN.

We also investigated the attention sink rate across models, defined as the proportion of attention heads where the first token attracts at least 30% of overall attention. For the original model, the sink rate was 55.3% [53.1%, 58.1%] (95% CI), which dropped to 45.3% [42.0%, 48.5%] for our LN-free variant. Interestingly, while this represents a notable reduction in sink rate, it is not proportional to the reduction we observed in L2 norms. This suggests that the relationship between relative token norm magnitudes and attention sink behavior is likely complex, with attention mechanisms potentially maintaining some degree of positional bias toward the first token even when its norm is substantially reduced.

This effect is likely due to the constant linear scaling applied by FakeLN. In models with LN, residual stream vectors are scaled by their individual standard deviations, meaning components are trained to operate under normalized input conditions. Once LN is removed, this normalization is no longer enforced. To compensate, the model appears to adapt by reducing variability in token norms, such as between the first token and the rest of the sequence. Our auxiliary loss further encourages norm consistency by explicitly penalizing variation across positions, however, we did observe this fundamental change in norm behavior even in experiments without this loss term.

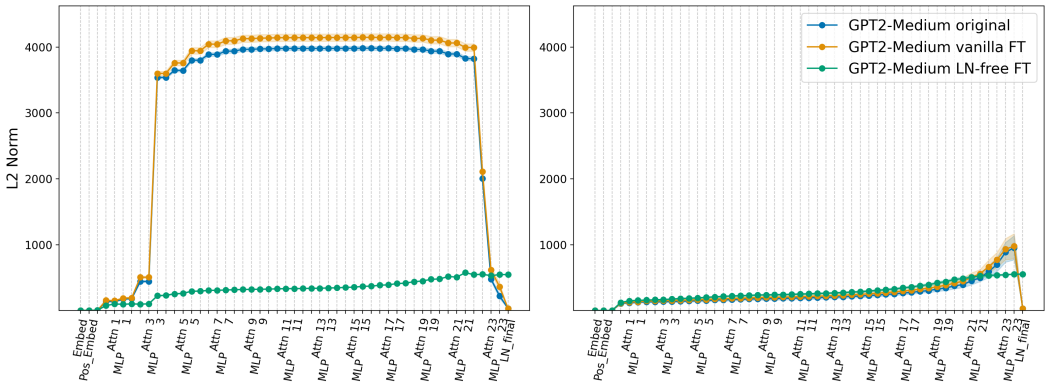

Figure 3: L2 norm growth for first position tokens (left) versus other positions tokens (right) for GPT-2 Medium models. First token norms significant deviate from norms at other positions for models trained with LN. LN-free model treats first token norm similarly to other positions.

5.4 Confidence neurons are neutered in LN-free models

When developing our LN-free model variants, we observed a consistent pattern: models exhibited significant overconfidence compared to their original counterparts. For GPT-2 Medium, the average entropy of the output distribution decreased from 2.86 [2.86, 2.87] (95% CI) in the original model to 2.53 [2.52, 2.54] in the LN-free version. Correspondingly, the expected calibration error, defined as the average absolute difference between the predicted confidence and accuracy, increased from 0.0019 [0.018, 0.020] to 0.034 [0.033, 0.035]. Motivated by these observations, we investigated how the recently discovered "confidence neurons" (also referred to as "entropy neurons") [Katz and Belinkov, 2023, Gurnee et al., 2024, Stolfo et al., 2024] in the final MLP layer were affected by our LN removal strategy.

Following Stolfo et al. [2024], we define confidence neurons as neurons in the final MLP with (a) a high weight norm, and (b) a uniform impact on all output logits. We detail how confidence neurons were identified and further analysis in Appendix G. We identified the same top-3 confidence neurons (1083, 1108, 3144) in GPT-2 Medium original, vanilla FT, and LN-free. To measure their importance in each model, we conducted mean ablations on 1,000 sequences consisting of 512 tokens in The Pile-filtered. For each neuron i, we replaced its input activation with its mean value across the dataset ($x_i \rightarrow \mathbb{E}[x_i]$). This intervention removes the neuron's contextual information while maintaining its average contribution. Figure 4 highlights the absolute change in cross-entropy loss when mean ablating each neuron. In the GPT-2 Medium original, all three neurons increase CE loss when ablated, with neuron 3144 showing the largest effect. In contrast, the impact is completely eliminated in LN-free model. This confirms that linearizing LN completely disables entropy neurons in the final MLP layer, further supporting previous work that identified LN's non-linearity as their primary enabling mechanism [Stolfo et al., 2024]. We also observed a decrease in the effectiveness of confidence neurons in our vanilla FT model, likely due to our fine-tuning hyperparameters, and is discussed further in Appendix G.

6 Discussion

6.1 Limitations

We successfully remove LN from all GPT-2 models. Here, we want to highlight common issues and possible limitations of this process. We find that the fine-tuning process when LNs are partially removed is, as expected, less stable. We find that the training loss can spike to high values on some inputs, which sometimes causes the training run to fail (irrecoverably high loss). A common failure we observed are exploding gradients, which most often occur during LN^l_v removal. Instabilities usually appear as a cascade of increasing gradient norms or exploding gradients in a single step.

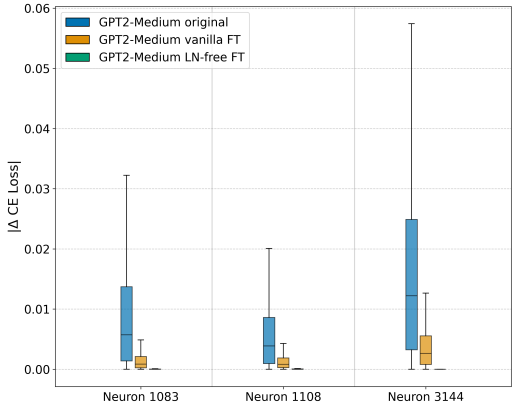

Figure 4: Absolute change in cross-entropy (CE) when ablating top-3 confidence neurons in GPT-2 Medium models. GPT-2 Medium original demonstrates a significant change in CE loss upon ablating, effect is significantly dampened in vanilla FT, and completely disappears in LN-free.

While our LN-removal strategies developed on GPT-2 Small and Medium largely transfer to the Large and XL models, they required significant hyperparameter tuning, which was computationally expensive. Additionally, an early version of our protocol without auxiliary loss worked for GPT-2 Small, but did not scale to larger models, suggesting that protocols don't always generalize across models.

As highlighted in Section 5.4, all of our LN-free models exhibit overconfidence compared to their LN counterparts. While our experiments demonstrate that removing LN effectively neutralizes confidence neurons, the magnitude of the observed increase in overconfidence suggests additional contributing factors. It's possible that without the normalizing effect of standard LN, attention, and MLP components must now handle greater variability in residual stream inputs, potentially compromising their ability to contribute to appropriate uncertainty quantification.

6.2 Future work

More models: We focused primarily on GPT-2 models, due to their ubiquity in the interpretability community. In the future, we would like to expand our LN removal protocol to more recent models.

Parameter efficient fine-tuning: So far we used full fine-tuning. While this was feasible for GPT-2 sized models, we want to explore parameter efficient fine-tuning strategies in the future.

Further protocol optimization: We noticed that the gap between removing the LN in different layers can be reduced for LN^l_{qk} and LN^l_{MLP}; in fact some experimental runs showed that we could remove those instances of LN in all layers simultaneously (only LN^l_{v} always required gaps).

Circuits interpretability: Attempts to create a sparse computational graph to represent a neural network are hindered by LN. It would be interesting to see if techniques like Marks et al. [2024] benefit from removing LN layers.

7 Conclusions

We showed that layer normalization can be gradually removed from transformer models with minimal performance loss using a fine-tuning procedure, demonstrating this on all GPT-2 models (and Pythia-70M). We detailed our procedure and the strategies used to address hyperparameter sensitivity. Applying interpretability techniques, we found that in LN-free models DLA becomes an exact estimate of DE and first-token residual norms become comparable to those at other positions. Surprisingly, attribution patching does not improve in LN-free models, suggesting its limitations stem from other nonlinearities. Finally, we showed that LN-free models lack operational entropy neurons, contributing towards the more generally observed trend of model overconfidence. Open-sourcing the models, we hope to contribute to mechanistic interpretability research.

References

Emmanuel Ameisen, Jack Lindsey, Adam Pearce, Wes Gurnee, Nicholas L. Turner, Brian Chen, Craig Citro, David Abrahams, Shan Carter, Basil Hosmer, Jonathan Marcus, Michael Sklar, Adly Templeton, Trenton Bricken, Callum McDougall, Hoagy Cunningham, Thomas Henighan, Adam Jermyn, Andy Jones, Andrew Persic, Zhenyi Qi, T. Ben Thompson, Sam Zimmerman, Kelley Rivoire, Thomas Conerly, Chris Olah, and Joshua Batson. Circuit tracing: Revealing computational graphs in language models. *Transformer Circuits Thread*, 2025. URL `https://transformer-circuits.pub/2025/attribution-graphs/methods.html`.

Jimmy Lei Ba, Jamie Ryan Kiros, and Geoffrey E. Hinton. Layer normalization, 2016.

Federico Barbero, Alvaro Arroyo, Xiangming Gu, Christos Perivolaropoulos, Michael Bronstein, Petar Veličković, and Razvan Pascanu. Why do LLMs attend to the first token? *arXiv preprint arXiv:2504.02732*, 2025.

Stella Biderman, Hailey Schoelkopf, Quentin Anthony, Herbie Bradley, Kyle O'Brien, Eric Hallahan, Mohammad Aflah Khan, Shivanshu Purohit, USVSN Sai Prashanth, Edward Raff, et al. Pythia: A suite for analyzing large language models across training and scaling. *arXiv preprint arXiv:2304.01373*, 2023.

Yonatan Bisk, Rowan Zellers, Jianfeng Gao, Yejin Choi, et al. Piqa: Reasoning about physical commonsense in natural language. In *Proceedings of the AAAI conference on artificial intelligence*, volume 34, pages 7432–7439, 2020.

Trenton Bricken, Adly Templeton, Joshua Batson, Brian Chen, Adam Jermyn, Tom Conerly, Nick Turner, Cem Anil, Carson Denison, Amanda Askell, Robert Lasenby, Yifan Wu, Shauna Kravec, Nicholas Schiefer, Tim Maxwell, Nicholas Joseph, Zac Hatfield-Dodds, Alex Tamkin, Karina Nguyen, Brayden McLean, Josiah E Burke, Tristan Hume, Shan Carter, Tom Henighan, and Christopher Olah. Towards monosemanticity: Decomposing language models with dictionary learning. *Transformer Circuits Thread*, 2023. https://transformer-circuits.pub/2023/monosemantic-features/index.html.

Lucius Bushnaq, Stefan Heimersheim, Nicholas Goldowsky-Dill, Dan Braun, Jake Mendel, Kaarel Hänni, Avery Griffin, Jörn Stöhler, Magdalena Wache, and Marius Hobbhahn. The local interaction basis: Identifying computationally-relevant and sparsely interacting features in neural networks. *arXiv preprint arXiv:2405.10928*, 2024.

Christopher Clark, Kenton Lee, Ming-Wei Chang, Tom Kwiatkowski, Michael Collins, and Kristina Toutanova. Boolq: Exploring the surprising difficulty of natural yes/no questions. *arXiv preprint arXiv:1905.10044*, 2019.

Nelson Elhage, Neel Nanda, Catherine Olsson, Tom Henighan, Nicholas Joseph, Ben Mann, Amanda Askell, Yuntao Bai, Anna Chen, Tom Conerly, Nova DasSarma, Dawn Drain, Deep Ganguli, Zac Hatfield-Dodds, Danny Hernandez, Andy Jones, Jackson Kernion, Liane Lovitt, Kamal Ndousse, Dario Amodei, Tom Brown, Jack Clark, Jared Kaplan, Sam McCandlish, and Chris Olah. A mathematical framework for transformer circuits. *Transformer Circuits Thread*, 2021. https://transformer-circuits.pub/2021/framework/index.html.

Lucy Farnik, Tim Lawson, Conor Houghton, and Laurence Aitchison. Jacobian sparse autoencoders: Sparsify computations, not just activations. *arXiv preprint arXiv:2502.18147*, 2025.

Leo Gao, Stella Biderman, Sid Black, Laurence Golding, Travis Hoppe, Charles Foster, Jason Phang, Horace He, Anish Thite, Noa Nabeshima, et al. The pile: An 800gb dataset of diverse text for language modeling. *arXiv preprint arXiv:2101.00027*, 2020.

Atticus Geiger, Zhengxuan Wu, Christopher Potts, Thomas Icard, and Noah Goodman. Finding alignments between interpretable causal variables and distributed neural representations. In *Causal Learning and Reasoning*, pages 160–187. PMLR, 2024.

Gemini Team, Rohan Anil, Sebastian Borgeaud, Jean-Baptiste Alayrac, Jiahui Yu, Radu Soricut, Johan Schalkwyk, Andrew M. Dai, Anja Hauth, Katie Millican, David Silver, Melvin Johnson, Ioannis Antonoglou, Julian Schrittwieser, Amelia Glaese, Jilin Chen, Emily Pitler, Timothy

Lillicrap, Angeliki Lazaridou, Orhan Firat, James Molloy, Michael Isard, Paul R. Barham, Tom Hennigan, Benjamin Lee, Fabio Viola, Malcolm Reynolds, Yuanzhong Xu, Ryan Doherty, Eli Collins, Clemens Meyer, Eliza Rutherford, Erica Moreira, Kareem Ayoub, Megha Goel, Jack Krawczyk, Cosmo Du, Ed Chi, Heng-Tze Cheng, Eric Ni, Purvi Shah, Patrick Kane, Betty Chan, Manaal Faruqui, Aliaksei Severyn, Hanzhao Lin, YaGuang Li, Yong Cheng, Abe Ittycheriah, Mahdis Mahdieh, Mia Chen, Pei Sun, Dustin Tran, Sumit Bagri, Balaji Lakshminarayanan, Jeremiah Liu, Andras Orban, Fabian Güra, Hao Zhou, Xinying Song, Aurelien Boffy, Harish Ganapathy, Steven Zheng, HyunJeong Choe, Ágoston Weisz, Tao Zhu, Yifeng Lu, Siddharth Gopal, Jarrod Kahn, Maciej Kula, Jeff Pitman, Rushin Shah, Emanuel Taropa, Majd Al Merey, Martin Baeuml, Zhifeng Chen, Laurent El Shafey, Yujing Zhang, Olcan Sercinoglu, George Tucker, Enrique Piqueras, Maxim Krikun, Iain Barr, Nikolay Savinov, Ivo Danihelka, Becca Roelofs, Anaïs White, Anders Andreassen, Tamara von Glehn, Lakshman Yagati, Mehran Kazemi, Lucas Gonzalez, Misha Khalman, Jakub Sygnowski, Alexandre Frechette, Charlotte Smith, Laura Culp, Lev Proleev, Yi Luan, Xi Chen, James Lottes, Nathan Schucher, Federico Lebron, Alban Rrustemi, Natalie Clay, Phil Crone, Tomas Kocisky, Jeffrey Zhao, Bartek Perz, Dian Yu, Heidi Howard, Adam Bloniarz, Jack W. Rae, Han Lu, Laurent Sifre, Marcello Maggioni, Fred Alcober, Dan Garrette, Megan Barnes, Shantanu Thakoor, Jacob Austin, Gabriel Barth-Maron, William Wong, Rishabh Joshi, Rahma Chaabouni, Deeni Fatiha, Arun Ahuja, Gaurav Singh Tomar, Evan Senter, Martin Chadwick, Ilya Kornakov, Nithya Attaluri, Iñaki Iturrate, Ruibo Liu, Yunxuan Li, Sarah Cogan, Jeremy Chen, Chao Jia, Chenjie Gu, Qiao Zhang, Jordan Grimstad, Ale Jakse Hartman, Xavier Garcia, Thanumalayan Sankaranarayana Pillai, Jacob Devlin, Michael Laskin, Diego de Las Casas, Dasha Valter, Connie Tao, Lorenzo Blanco, Adrià Puigdomènech Badia, David Reitter, Mianna Chen, Jenny Brennan, Clara Rivera, Sergey Brin, Shariq Iqbal, Gabriela Surita, Jane Labanowski, Abhi Rao, Stephanie Winkler, Emilio Parisotto, Yiming Gu, Kate Olszewska, Ravi Addanki, Antoine Miech, Annie Louis, Denis Teplyashin, Geoff Brown, Elliot Catt, Jan Balaguer, Jackie Xiang, Pidong Wang, Zoe Ashwood, Anton Briukhov, Albert Webson, Sanjay Ganapathy, Smit Sanghavi, Ajay Kannan, Ming-Wei Chang, Axel Stjerngren, Josip Djolonga, Yuting Sun, Ankur Bapna, Matthew Aitchison, Pedram Pejman, Henryk Michalewski, Tianhe Yu, Cindy Wang, Juliette Love, Junwhan Ahn, Dawn Bloxwich, Kehang Han, Peter Humphreys, Thibault Sellam, James Bradbury, Varun Godbole, Sina Samangooei, Bogdan Damoc, Alex Kaskasoli, Sébastien M. R. Arnold, Vijay Vasudevan, Shubham Agrawal, Jason Riesa, Dmitry Lepikhin, Richard Tanburn, Srivatsan Srinivasan, Hyeontaek Lim, Sarah Hodkinson, Pranav Shyam, Johan Ferret, Steven Hand, Ankush Garg, Tom Le Paine, Jian Li, Yujia Li, Minh Giang, Alexander Neitz, Zaheer Abbas, Sarah York, Machel Reid, Elizabeth Cole, Aakanksha Chowdhery, Dipanjan Das, Dominika Rogozińska, Vitaliy Nikolaev, Pablo Sprechmann, Zachary Nado, Lukas Zilka, Flavien Prost, Luheng He, Marianne Monteiro, Gaurav Mishra, Chris Welty, Josh Newlan, Dawei Jia, Miltiadis Allamanis, Clara Huiyi Hu, Raoul de Liedekerke, Justin Gilmer, Carl Saroufim, Shruti Rijhwani, Shaobo Hou, Disha Shrivastava, Anirudh Baddepudi, Alex Goldin, Adnan Ozturel, Albin Cassirer, Yunhan Xu, Daniel Sohn, Devendra Sachan, Reinald Kim Amplayo, Craig Swanson, Dessie Petrova, Shashi Narayan, Arthur Guez, Siddhartha Brahma, Jessica Landon, Miteyan Patel, Ruizhe Zhao, Kevin Villela, Luyu Wang, Wenhao Jia, Matthew Rahtz, Mai Giménez, Legg Yeung, James Keeling, Petko Georgiev, Diana Mincu, Boxi Wu, Salem Haykal, Rachel Saputro, Kiran Vodrahalli, James Qin, Zeynep Cankara, Abhanshu Sharma, Nick Fernando, Will Hawkins, Behnam Neyshabur, Solomon Kim, Adrian Hutter, Priyanka Agrawal, Alex Castro-Ros, George van den Driessche, Tao Wang, Fan Yang, Shuo yiin Chang, Paul Komarek, Ross McIlroy, Mario Lučić, Guodong Zhang, Wael Farhan, Michael Sharman, Paul Natsev, Paul Michel, Yamini Bansal, Siyuan Qiao, Kris Cao, Siamak Shakeri, Christina Butterfield, Justin Chung, Paul Kishan Rubenstein, Shivani Agrawal, Arthur Mensch, Kedar Soparkar, Karel Lenc, Timothy Chung, Aedan Pope, Loren Maggiore, Jackie Kay, Priya Jhakra, Shibo Wang, Joshua Maynez, Mary Phuong, Taylor Tobin, Andrea Tacchetti, Maja Trebacz, Kevin Robinson, Yash Katariya, Sebastian Riedel, Paige Bailey, Kefan Xiao, Nimesh Ghelani, Lora Aroyo, Ambrose Slone, Neil Houlsby, Xuehan Xiong, Zhen Yang, Elena Gribovskaya, Jonas Adler, Mateo Wirth, Lisa Lee, Music Li, Thais Kagohara, Jay Pavagadhi, Sophie Bridgers, Anna Bortsova, Sanjay Ghemawat, Zafarali Ahmed, Tianqi Liu, Richard Powell, Vijay Bolina, Mariko Iinuma, Polina Zablotskaia, James Besley, Da-Woon Chung, Timothy Dozat, Ramona Comanescu, Xiance Si, Jeremy Greer, Guolong Su, Martin Polacek, Raphaël Lopez Kaufman, Simon Tokumine, Hexiang Hu, Elena Buchatskaya, Yingjie Miao, Mohamed Elhawaty, Aditya Siddhant, Nenad Tomasev, Jinwei Xing, Christina Greer, Helen Miller, Shereen Ashraf, Aurko Roy, Zizhao Zhang, Ada Ma, Angelos Filos, Milos Besta, Rory Blevins, Ted Klimenko, Chih-Kuan Yeh, Soravit Changpinyo, Jiaqi Mu, Oscar Chang, Mantas Pajarskas,

Carrie Muir, Vered Cohen, Charline Le Lan, Krishna Haridasan, Amit Marathe, Steven Hansen, Sholto Douglas, Rajkumar Samuel, Mingqiu Wang, Sophia Austin, Chang Lan, Jiepu Jiang, Justin Chiu, Jaime Alonso Lorenzo, Lars Lowe Sjösund, Sébastien Cevey, Zach Gleicher, Thi Avrahami, Anudhyan Boral, Hansa Srinivasan, Vittorio Selo, Rhys May, Konstantinos Aisopos, Léonard Hussenot, Livio Baldini Soares, Kate Baumli, Michael B. Chang, Adrià Recasens, Ben Caine, Alexander Pritzel, Filip Pavetic, Fabio Pardo, Anita Gergely, Justin Frye, Vinay Ramasesh, Dan Horgan, Kartikeya Badola, Nora Kassner, Subhrajit Roy, Ethan Dyer, Víctor Campos Campos, Alex Tomala, Yunhao Tang, Dalia El Badawy, Elspeth White, Basil Mustafa, Oran Lang, Abhishek Jindal, Sharad Vikram, Zhitao Gong, Sergi Caelles, Ross Hemsley, Gregory Thornton, Fangxiaoyu Feng, Wojciech Stokowiec, Ce Zheng, Phoebe Thacker, Çağlar Ünlü, Zhishuai Zhang, Mohammad Saleh, James Svensson, Max Bileschi, Piyush Patil, Ankesh Anand, Roman Ring, Katerina Tsihlas, Arpi Vezer, Marco Selvi, Toby Shevlane, Mikel Rodriguez, Tom Kwiatkowski, Samira Daruki, Keran Rong, Allan Dafoe, Nicholas FitzGerald, Keren Gu-Lemberg, Mina Khan, Lisa Anne Hendricks, Marie Pellat, Vladimir Feinberg, James Cobon-Kerr, Tara Sainath, Maribeth Rauh, Sayed Hadi Hashemi, Richard Ives, Yana Hasson, Eric Noland, Yuan Cao, Nathan Byrd, Le Hou, Qingze Wang, Thibault Sottiaux, Michela Paganini, Jean-Baptiste Lespiau, Alexandre Moufarek, Samer Hassan, Kaushik Shivakumar, Joost van Amersfoort, Amol Mandhane, Pratik Joshi, Anirudh Goyal, Matthew Tung, Andrew Brock, Hannah Sheahan, Vedant Misra, Cheng Li, Nemanja Rakićević, Mostafa Dehghani, Fangyu Liu, Sid Mittal, Junhyuk Oh, Seb Noury, Eren Sezener, Fantine Huot, Matthew Lamm, Nicola De Cao, Charlie Chen, Sidharth Mudgal, Romina Stella, Kevin Brooks, Gautam Vasudevan, Chenxi Liu, Mainak Chain, Nivedita Melinkeri, Aaron Cohen, Venus Wang, Kristie Seymore, Sergey Zubkov, Rahul Goel, Summer Yue, Sai Krishnakumaran, Brian Albert, Nate Hurley, Motoki Sano, Anhad Mohananey, Jonah Joughin, Egor Filonov, Tomasz Kępa, Yomna Eldawy, Jiawern Lim, Rahul Rishi, Shirin Badiezadegan, Taylor Bos, Jerry Chang, Sanil Jain, Sri Gayatri Sundara Padmanabhan, Subha Puttagunta, Kalpesh Krishna, Leslie Baker, Norbert Kalb, Vamsi Bedapudi, Adam Kurzrok, Shuntong Lei, Anthony Yu, Oren Litvin, Xiang Zhou, Zhichun Wu, Sam Sobell, Andrea Siciliano, Alan Papir, Robby Neale, Jonas Bragagnolo, Tej Toor, Tina Chen, Valentin Anklin, Feiran Wang, Richie Feng, Milad Gholami, Kevin Ling, Lijuan Liu, Jules Walter, Hamid Moghaddam, Arun Kishore, Jakub Adamek, Tyler Mercado, Jonathan Mallinson, Siddhinita Wandekar, Stephen Cagle, Eran Ofek, Guillermo Garrido, Clemens Lombriser, Maksim Mukha, Botu Sun, Hafeezul Rahman Mohammad, Josip Matak, Yadi Qian, Vikas Peswani, Pawel Janus, Quan Yuan, Leif Schelin, Oana David, Ankur Garg, Yifan He, Oleksii Duzhyi, Anton Älgmyr, Timothée Lottaz, Qi Li, Vikas Yadav, Luyao Xu, Alex Chinien, Rakesh Shivanna, Aleksandr Chuklin, Josie Li, Carrie Spadine, Travis Wolfe, Kareem Mohamed, Subhabrata Das, Zihang Dai, Kyle He, Daniel von Dincklage, Shyam Upadhyay, Akanksha Maurya, Luyan Chi, Sebastian Krause, Khalid Salama, Pam G Rabinovitch, Pavan Kumar Reddy M, Aarush Selvan, Mikhail Dektiarev, Golnaz Ghiasi, Erdem Guven, Himanshu Gupta, Boyi Liu, Deepak Sharma, Idan Heimlich Shtacher, Shachi Paul, Oscar Akerlund, François-Xavier Aubet, Terry Huang, Chen Zhu, Eric Zhu, Elico Teixeira, Matthew Fritze, Francesco Bertolini, Liana-Eleonora Marinescu, Martin Bölle, Dominik Paulus, Khyatti Gupta, Tejasi Latkar, Max Chang, Jason Sanders, Roopa Wilson, Xuewei Wu, Yi-Xuan Tan, Lam Nguyen Thiet, Tulsee Doshi, Sid Lall, Swaroop Mishra, Wanming Chen, Thang Luong, Seth Benjamin, Jasmine Lee, Ewa Andrejczuk, Dominik Rabiej, Vipul Ranjan, Krzysztof Styrc, Pengcheng Yin, Jon Simon, Malcolm Rose Harriott, Mudit Bansal, Alexei Robsky, Geoff Bacon, David Greene, Daniil Mirylenka, Chen Zhou, Obaid Sarvana, Abhimanyu Goyal, Samuel Andermatt, Patrick Siegler, Ben Horn, Assaf Israel, Francesco Pongetti, Chih-Wei "Louis" Chen, Marco Selvatici, Pedro Silva, Kathie Wang, Jackson Tolins, Kelvin Guu, Roey Yogev, Xiaochen Cai, Alessandro Agostini, Maulik Shah, Hung Nguyen, Noah Ó Donnaile, Sébastien Pereira, Linda Friso, Adam Stambler, Adam Kurzrok, Chenkai Kuang, Yan Romanikhin, Mark Geller, ZJ Yan, Kane Jang, Cheng-Chun Lee, Wojciech Fica, Eric Malmi, Qijun Tan, Dan Banica, Daniel Balle, Ryan Pham, Yanping Huang, Diana Avram, Hongzhi Shi, Jasjot Singh, Chris Hidey, Niharika Ahuja, Pranab Saxena, Dan Dooley, Srividya Pranavi Potharaju, Eileen O'Neill, Anand Gokulchandran, Ryan Foley, Kai Zhao, Mike Dusenberry, Yuan Liu, Pulkit Mehta, Ragha Kotikalapudi, Chalence Safranek-Shrader, Andrew Goodman, Joshua Kessinger, Eran Globen, Prateek Kolhar, Chris Gorgolewski, Ali Ibrahim, Yang Song, Ali Eichenbaum, Thomas Brovelli, Sahitya Potluri, Preethi Lahoti, Cip Baetu, Ali Ghorbani, Charles Chen, Andy Crawford, Shalini Pal, Mukund Sridhar, Petru Gurita, Asier Mujika, Igor Petrovski, Pierre-Louis Cedoz, Chenmei Li, Shiyuan Chen, Niccolò Dal Santo, Siddharth Goyal, Jitesh Punjabi, Karthik Kappaganthu, Chester Kwak, Pallavi LV, Sarmishta Velury, Himadri Choudhury, Jamie Hall, Premal Shah, Ricardo Figueira, Matt Thomas, Minjie Lu, Ting Zhou, Chintu Kumar, Thomas Jurdi, Sharat Chikkerur,

Yenai Ma, Adams Yu, Soo Kwak, Victor Ähdel, Sujeevan Rajayogam, Travis Choma, Fei Liu, Aditya Barua, Colin Ji, Ji Ho Park, Vincent Hellendoorn, Alex Bailey, Taylan Bilal, Huanjie Zhou, Mehrdad Khatir, Charles Sutton, Wojciech Rzadkowski, Fiona Macintosh, Konstantin Shagin, Paul Medina, Chen Liang, Jinjing Zhou, Pararth Shah, Yingying Bi, Attila Dankovics, Shipra Banga, Sabine Lehmann, Marissa Bredesen, Zifan Lin, John Eric Hoffmann, Jonathan Lai, Raynald Chung, Kai Yang, Nihal Balani, Arthur Bražinskas, Andrei Sozanschi, Matthew Hayes, Héctor Fernández Alcalde, Peter Makarov, Will Chen, Antonio Stella, Liselotte Snijders, Michael Mandl, Ante Kärrman, Paweł Nowak, Xinyi Wu, Alex Dyck, Krishnan Vaidyanathan, Raghavender R, Jessica Mallet, Mitch Rudominer, Eric Johnston, Sushil Mittal, Akhil Udathu, Janara Christensen, Vishal Verma, Zach Irving, Andreas Santucci, Gamaleldin Elsayed, Elnaz Davoodi, Marin Georgiev, Ian Tenney, Nan Hua, Geoffrey Cideron, Edouard Leurent, Mahmoud Alnahlawi, Ionut Georgescu, Nan Wei, Ivy Zheng, Dylan Scandinaro, Heinrich Jiang, Jasper Snoek, Mukund Sundararajan, Xuezhi Wang, Zack Ontiveros, Itay Karo, Jeremy Cole, Vinu Rajashekhar, Lara Tumeh, Eyal Ben-David, Rishub Jain, Jonathan Uesato, Romina Datta, Oskar Bunyan, Shimu Wu, John Zhang, Piotr Stanczyk, Ye Zhang, David Steiner, Subhajit Naskar, Michael Azzam, Matthew Johnson, Adam Paszke, Chung-Cheng Chiu, Jaume Sanchez Elias, Afroz Mohiuddin, Faizan Muhammad, Jin Miao, Andrew Lee, Nino Vieillard, Jane Park, Jiageng Zhang, Jeff Stanway, Drew Garmon, Abhijit Karmarkar, Zhe Dong, Jong Lee, Aviral Kumar, Luowei Zhou, Jonathan Evens, William Isaac, Geoffrey Irving, Edward Loper, Michael Fink, Isha Arkatkar, Nanxin Chen, Izhak Shafran, Ivan Petrychenko, Zhe Chen, Johnson Jia, Anselm Levskaya, Zhenkai Zhu, Peter Grabowski, Yu Mao, Alberto Magni, Kaisheng Yao, Javier Snaider, Norman Casagrande, Evan Palmer, Paul Suganthan, Alfonso Castaño, Irene Giannoumis, Wooyeol Kim, Mikołaj Rybiński, Ashwin Sreevatsa, Jennifer Prendki, David Soergel, Adrian Goedeckemeyer, Willi Gierke, Mohsen Jafari, Meenu Gaba, Jeremy Wiesner, Diana Gage Wright, Yawen Wei, Harsha Vashisht, Yana Kulizhskaya, Jay Hoover, Maigo Le, Lu Li, Chimezie Iwuanyanwu, Lu Liu, Kevin Ramirez, Andrey Khorlin, Albert Cui, Tian LIN, Marcus Wu, Ricardo Aguilar, Keith Pallo, Abhishek Chakladar, Ginger Perng, Elena Allica Abellan, Mingyang Zhang, Ishita Dasgupta, Nate Kushman, Ivo Penchev, Alena Repina, Xihui Wu, Tom van der Weide, Priya Ponnapalli, Caroline Kaplan, Jiri Simsa, Shuangfeng Li, Olivier Dousse, Fan Yang, Jeff Piper, Nathan Ie, Rama Pasumarthi, Nathan Lintz, Anitha Vijayakumar, Daniel Andor, Pedro Valenzuela, Minnie Lui, Cosmin Paduraru, Daiyi Peng, Katherine Lee, Shuyuan Zhang, Somer Greene, Duc Dung Nguyen, Paula Kurylowicz, Cassidy Hardin, Lucas Dixon, Lili Janzer, Kiam Choo, Ziqiang Feng, Biao Zhang, Achintya Singhal, Dayou Du, Dan McKinnon, Natasha Antropova, Tolga Bolukbasi, Orgad Keller, David Reid, Daniel Finchelstein, Maria Abi Raad, Remi Crocker, Peter Hawkins, Robert Dadashi, Colin Gaffney, Ken Franko, Anna Bulanova, Rémi Leblond, Shirley Chung, Harry Askham, Luis C. Cobo, Kelvin Xu, Felix Fischer, Jun Xu, Christina Sorokin, Chris Alberti, Chu-Cheng Lin, Colin Evans, Alek Dimitriev, Hannah Forbes, Dylan Banarse, Zora Tung, Mark Omernick, Colton Bishop, Rachel Sterneck, Rohan Jain, Jiawei Xia, Ehsan Amid, Francesco Piccinno, Xingyu Wang, Praseem Banzal, Daniel J. Mankowitz, Alex Polozov, Victoria Krakovna, Sasha Brown, MohammadHossein Bateni, Dennis Duan, Vlad Firoiu, Meghana Thotakuri, Tom Natan, Matthieu Geist, Ser tan Girgin, Hui Li, Jiayu Ye, Ofir Roval, Reiko Tojo, Michael Kwong, James Lee-Thorp, Christopher Yew, Danila Sinopalnikov, Sabela Ramos, John Mellor, Abhishek Sharma, Kathy Wu, David Miller, Nicolas Sonnerat, Denis Vnukov, Rory Greig, Jennifer Beattie, Emily Caveness, Libin Bai, Julian Eisenschlos, Alex Korchemniy, Tomy Tsai, Mimi Jasarevic, Weize Kong, Phuong Dao, Zeyu Zheng, Frederick Liu, Fan Yang, Rui Zhu, Tian Huey Teh, Jason Sanmiya, Evgeny Gladchenko, Nejc Trdin, Daniel Toyama, Evan Rosen, Sasan Tavakkol, Linting Xue, Chen Elkind, Oliver Woodman, John Carpenter, George Papamakarios, Rupert Kemp, Sushant Kafle, Tanya Grunina, Rishika Sinha, Alice Talbert, Diane Wu, Denese Owusu-Afriyie, Cosmo Du, Chloe Thornton, Jordi Pont-Tuset, Pradyumna Narayana, Jing Li, Saaber Fatehi, John Wieting, Omar Ajmeri, Benigno Uria, Yeongil Ko, Laura Knight, Amélie Héliou, Ning Niu, Shane Gu, Chenxi Pang, Yeqing Li, Nir Levine, Ariel Stolovich, Rebeca Santamaria-Fernandez, Sonam Goenka, Wenny Yustalim, Robin Strudel, Ali Elqursh, Charlie Deck, Hyo Lee, Zonglin Li, Kyle Levin, Raphael Hoffmann, Dan Holtmann-Rice, Olivier Bachem, Sho Arora, Christy Koh, Soheil Hassas Yeganeh, Siim Põder, Mukarram Tariq, Yanhua Sun, Lucian Ionita, Mojtaba Seyedhosseini, Pouya Tafti, Zhiyu Liu, Anmol Gulati, Jasmine Liu, Xinyu Ye, Bart Chrzaszcz, Lily Wang, Nikhil Sethi, Tianrun Li, Ben Brown, Shreya Singh, Wei Fan, Aaron Parisi, Joe Stanton, Vinod Koverkathu, Christopher A. Choquette-Choo, Yunjie Li, TJ Lu, Abe Ittycheriah, Prakash Shroff, Mani Varadarajan, Sanaz Bahargam, Rob Willoughby, David Gaddy, Guillaume Desjardins, Marco Cornero, Brona Robenek, Bhavishya Mittal, Ben Albrecht, Ashish Shenoy, Fedor Moiseev, Henrik Jacobsson, Alireza Ghaffarkhah, Morgane Rivière, Alanna

Walton, Clément Crepy, Alicia Parrish, Zongwei Zhou, Clement Farabet, Carey Radebaugh, Praveen Srinivasan, Claudia van der Salm, Andreas Fidjeland, Salvatore Scellato, Eri Latorre-Chimoto, Hanna Klimczak-Plucińska, David Bridson, Dario de Cesare, Tom Hudson, Piermaria Mendolicchio, Lexi Walker, Alex Morris, Matthew Mauger, Alexey Guseynov, Alison Reid, Seth Odoom, Lucia Loher, Victor Cotruta, Madhavi Yenugula, Dominik Grewe, Anastasia Petrushkina, Tom Duerig, Antonio Sanchez, Steve Yadlowsky, Amy Shen, Amir Globerson, Lynette Webb, Sahil Dua, Dong Li, Surya Bhupatiraju, Dan Hurt, Haroon Qureshi, Ananth Agarwal, Tomer Shani, Matan Eyal, Anuj Khare, Shreyas Rammohan Belle, Lei Wang, Chetan Tekur, Mihir Sanjay Kale, Jinliang Wei, Ruoxin Sang, Brennan Saeta, Tyler Liechty, Yi Sun, Yao Zhao, Stephan Lee, Pandu Nayak, Doug Fritz, Manish Reddy Vuyyuru, John Aslanides, Nidhi Vyas, Martin Wicke, Xiao Ma, Evgenii Eltyshev, Nina Martin, Hardie Cate, James Manyika, Keyvan Amiri, Yelin Kim, Xi Xiong, Kai Kang, Florian Luisier, Nilesh Tripuraneni, David Madras, Mandy Guo, Austin Waters, Oliver Wang, Joshua Ainslie, Jason Baldridge, Han Zhang, Garima Pruthi, Jakob Bauer, Feng Yang, Riham Mansour, Jason Gelman, Yang Xu, George Polovets, Ji Liu, Honglong Cai, Warren Chen, XiangHai Sheng, Emily Xue, Sherjil Ozair, Christof Angermueller, Xiaowei Li, Anoop Sinha, Weiren Wang, Julia Wiesinger, Emmanouil Koukoumidis, Yuan Tian, Anand Iyer, Madhu Gurumurthy, Mark Goldenson, Parashar Shah, MK Blake, Hongkun Yu, Anthony Urbanowicz, Jennimaria Palomaki, Chrisantha Fernando, Ken Durden, Harsh Mehta, Nikola Momchev, Elahe Rahimtoroghi, Maria Georgaki, Amit Raul, Sebastian Ruder, Morgan Redshaw, Jinhyuk Lee, Denny Zhou, Komal Jalan, Dinghua Li, Blake Hechtman, Parker Schuh, Milad Nasr, Kieran Milan, Vladimir Mikulik, Juliana Franco, Tim Green, Nam Nguyen, Joe Kelley, Aroma Mahendru, Andrea Hu, Joshua Howland, Ben Vargas, Jeffrey Hui, Kshitij Bansal, Vikram Rao, Rakesh Ghiya, Emma Wang, Ke Ye, Jean Michel Sarr, Melanie Moranski Preston, Madeleine Elish, Steve Li, Aakash Kaku, Jigar Gupta, Ice Pasupat, Da-Cheng Juan, Milan Someswar, Tejvi M., Xinyun Chen, Aida Amini, Alex Fabrikant, Eric Chu, Xuanyi Dong, Amruta Muthal, Senaka Buthpitiya, Sarthak Jauhari, Nan Hua, Urvashi Khandelwal, Ayal Hitron, Jie Ren, Larissa Rinaldi, Shahar Drath, Avigail Dabush, Nan-Jiang Jiang, Harshal Godhia, Uli Sachs, Anthony Chen, Yicheng Fan, Hagai Taitelbaum, Hila Noga, Zhuyun Dai, James Wang, Chen Liang, Jenny Hamer, Chun-Sung Ferng, Chenel Elkind, Aviel Atias, Paulina Lee, Vít Listík, Mathias Carlen, Jan van de Kerkhof, Marcin Pikus, Krunoslav Zaher, Paul Müller, Sasha Zykova, Richard Stefanec, Vitaly Gatsko, Christoph Hirnschall, Ashwin Sethi, Xingyu Federico Xu, Chetan Ahuja, Beth Tsai, Anca Stefanoiu, Bo Feng, Keshav Dhandhania, Manish Katyal, Akshay Gupta, Atharva Parulekar, Divya Pitta, Jing Zhao, Vivaan Bhatia, Yashodha Bhavnani, Omar Alhadlaq, Xiaolin Li, Peter Danenberg, Dennis Tu, Alex Pine, Vera Filippova, Abhipso Ghosh, Ben Limonchik, Bhargava Urala, Chaitanya Krishna Lanka, Derik Clive, Yi Sun, Edward Li, Hao Wu, Kevin Hongtongsak, Ianna Li, Kalind Thakkar, Kuanysh Omarov, Kushal Majmundar, Michael Alverson, Michael Kucharski, Mohak Patel, Mudit Jain, Maksim Zabelin, Paolo Pelagatti, Rohan Kohli, Saurabh Kumar, Joseph Kim, Swetha Sankar, Vineet Shah, Lakshmi Ramachandruni, Xiangkai Zeng, Ben Bariach, Laura Weidinger, Tu Vu, Alek Andreev, Antoine He, Kevin Hui, Sheleem Kashem, Amar Subramanya, Sissie Hsiao, Demis Hassabis, Koray Kavukcuoglu, Adam Sadovsky, Quoc Le, Trevor Strohman, Yonghui Wu, Slav Petrov, Jeffrey Dean, and Oriol Vinyals. Gemini: A family of highly capable multimodal models, 2024. URL https://arxiv.org/abs/2312.11805.

Aaron Gokaslan and Vanya Cohen. Openwebtext corpus. http://Skylion007.github.io/OpenWebTextCorpus, 2019.

Akshat Gupta, Atahan Ozdemir, and Gopala Anumanchipalli. Geometric interpretation of layer normalization and a comparative analysis with rmsnorm, 2025.

Wes Gurnee, Theo Horsley, Zifan Carl Guo, Tara Rezaei Kheirkhah, Qinyi Sun, Will Hathaway, Neel Nanda, and Dimitris Bertsimas. Universal neurons in gpt2 language models. *Transactions on Machine Learning Research*, 2024.

Stefan Heimersheim and Neel Nanda. How to use and interpret activation patching. *arXiv preprint arXiv:2404.15255*, 2024.

Sergey Ioffe and Christian Szegedy. Batch normalization: Accelerating deep network training by reducing internal covariate shift. In Francis Bach and David Blei, editors, *Proceedings of the 32nd International Conference on Machine Learning*, volume 37 of *Proceedings of Machine Learning Research*, pages 448–456, Lille, France, 07–09 Jul 2015. PMLR. URL https://proceedings.mlr.press/v37/ioffe15.html.

Shahar Katz and Yonatan Belinkov. Visit: Visualizing and interpreting the semantic information flow of transformers. In *Findings of the Association for Computational Linguistics: EMNLP 2023*, pages 14094–14113, 2023.

Connor Kissane, Robert Krzyzanowski, Arthur Conmy, and Neel Nanda. Sparse autoencoders work on attention layer outputs, Jan 2024. URL https://www.alignmentforum.org/posts/DtdzGwFh9dCfsekZZ/sparse-autoencoders-work-on-attention-layer-outputs.

Jack Lindsey, Wes Gurnee, Emmanuel Ameisen, Brian Chen, Adam Pearce, Nicholas L. Turner, Craig Citro, David Abrahams, Shan Carter, Basil Hosmer, Jonathan Marcus, Michael Sklar, Adly Templeton, Trenton Bricken, Callum McDougall, Hoagy Cunningham, Thomas Henighan, Adam Jermyn, Andy Jones, Andrew Persic, Zhenyi Qi, T. Ben Thompson, Sam Zimmerman, Kelley Rivoire, Thomas Conerly, Chris Olah, and Joshua Batson. On the biology of a large language model. *Transformer Circuits Thread*, 2025. URL https://transformer-circuits.pub/2025/attribution-graphs/biology.html.

Samuel Marks, Can Rager, Eric J Michaud, Yonatan Belinkov, David Bau, and Aaron Mueller. Sparse feature circuits: Discovering and editing interpretable causal graphs in language models. *arXiv preprint arXiv:2403.19647*, 2024.

Callum McDougall, Arthur Conmy, Cody Rushing, Thomas McGrath, and Neel Nanda. Copy Suppression: Comprehensively Understanding an Attention Head. *arXiv e-prints*, art. arXiv:2310.04625, October 2023. doi: 10.48550/arXiv.2310.04625.

Kevin Meng, David Bau, Alex Andonian, and Yonatan Belinkov. Locating and editing factual associations in GPT. *Advances in Neural Information Processing Systems*, 36, 2022. arXiv:2202.05262.

Noa Nabeshima. Tinymodel: A tinystories lm with saes and transcoders, 2024. URL https://github.com/noanabeshima/tinymodel. Accessed: 2025-05-15.

Neel Nanda. Attribution patching: Activation patching at industrial scale, Mar 2023a. URL https://www.alignmentforum.org/posts/gtLLBhzQTG6nKTeCZ/attribution-patching-activation-patching-at-industrial-scale.

Neel Nanda. Exploratory analysis demo (transformerlens). https://colab.research.google.com/github/neelnanda-io/TransformerLens/blob/main/demos/Exploratory_Analysis_Demo.ipynb, 2023b.

Neel Nanda and Joseph Bloom. Transformerlens. https://github.com/TransformerLensOrg/TransformerLens, 2022.

nostalgebraist. interpreting gpt: the logit lens, Aug 2020. URL https://www.alignmentforum.org/posts/AcKRB8wDpdaN6v6ru/interpreting-gpt-the-logit-lens.

OpenAI, Josh Achiam, Steven Adler, Sandhini Agarwal, Lama Ahmad, Ilge Akkaya, Florencia Leoni Aleman, Diogo Almeida, Janko Altenschmidt, Sam Altman, Shyamal Anadkat, Red Avila, Igor Babuschkin, Suchir Balaji, Valerie Balcom, Paul Baltescu, Haiming Bao, Mohammad Bavarian, Jeff Belgum, Irwan Bello, Jake Berdine, Gabriel Bernadett-Shapiro, Christopher Berner, Lenny Bogdonoff, Oleg Boiko, Madelaine Boyd, Anna-Luisa Brakman, Greg Brockman, Tim Brooks, Miles Brundage, Kevin Button, Trevor Cai, Rosie Campbell, Andrew Cann, Brittany Carey, Chelsea Carlson, Rory Carmichael, Brooke Chan, Che Chang, Fotis Chantzis, Derek Chen, Sully Chen, Ruby Chen, Jason Chen, Mark Chen, Ben Chess, Chester Cho, Casey Chu, Hyung Won Chung, Dave Cummings, Jeremiah Currier, Yunxing Dai, Cory Decareaux, Thomas Degry, Noah Deutsch, Damien Deville, Arka Dhar, David Dohan, Steve Dowling, Sheila Dunning, Adrien Ecoffet, Atty Eleti, Tyna Eloundou, David Farhi, Liam Fedus, Niko Felix, Simón Posada Fishman, Juston Forte, Isabella Fulford, Leo Gao, Elie Georges, Christian Gibson, Vik Goel, Tarun Gogineni, Gabriel Goh, Rapha Gontijo-Lopes, Jonathan Gordon, Morgan Grafstein, Scott Gray, Ryan Greene, Joshua Gross, Shixiang Shane Gu, Yufei Guo, Chris Hallacy, Jesse Han, Jeff Harris, Yuchen He, Mike Heaton, Johannes Heidecke, Chris Hesse, Alan Hickey, Wade Hickey, Peter Hoeschele, Brandon Houghton, Kenny Hsu, Shengli Hu, Xin Hu, Joost Huizinga, Shantanu Jain, Shawn Jain, Joanne Jang, Angela Jiang, Roger Jiang, Haozhun Jin, Denny Jin, Shino Jomoto, Billie Jonn, Heewoo Jun, Tomer Kaftan, Łukasz Kaiser, Ali Kamali, Ingmar Kanitscheider, Nitish Shirish Keskar,

Tabarak Khan, Logan Kilpatrick, Jong Wook Kim, Christina Kim, Yongjik Kim, Jan Hendrik Kirchner, Jamie Kiros, Matt Knight, Daniel Kokotajlo, Łukasz Kondraciuk, Andrew Kondrich, Aris Konstantinidis, Kyle Kosic, Gretchen Krueger, Vishal Kuo, Michael Lampe, Ikai Lan, Teddy Lee, Jan Leike, Jade Leung, Daniel Levy, Chak Ming Li, Rachel Lim, Molly Lin, Stephanie Lin, Mateusz Litwin, Theresa Lopez, Ryan Lowe, Patricia Lue, Anna Makanju, Kim Malfacini, Sam Manning, Todor Markov, Yaniv Markovski, Bianca Martin, Katie Mayer, Andrew Mayne, Bob McGrew, Scott Mayer McKinney, Christine McLeavey, Paul McMillan, Jake McNeil, David Medina, Aalok Mehta, Jacob Menick, Luke Metz, Andrey Mishchenko, Pamela Mishkin, Vinnie Monaco, Evan Morikawa, Daniel Mossing, Tong Mu, Mira Murati, Oleg Murk, David Mély, Ashvin Nair, Reiichiro Nakano, Rajeev Nayak, Arvind Neelakantan, Richard Ngo, Hyeonwoo Noh, Long Ouyang, Cullen O'Keefe, Jakub Pachocki, Alex Paino, Joe Palermo, Ashley Pantuliano, Giambattista Parascandolo, Joel Parish, Emy Parparita, Alex Passos, Mikhail Pavlov, Andrew Peng, Adam Perelman, Filipe de Avila Belbute Peres, Michael Petrov, Henrique Ponde de Oliveira Pinto, Michael, Pokorny, Michelle Pokrass, Vitchyr H. Pong, Tolly Powell, Alethea Power, Boris Power, Elizabeth Proehl, Raul Puri, Alec Radford, Jack Rae, Aditya Ramesh, Cameron Raymond, Francis Real, Kendra Rimbach, Carl Ross, Bob Rotsted, Henri Roussez, Nick Ryder, Mario Saltarelli, Ted Sanders, Shibani Santurkar, Girish Sastry, Heather Schmidt, David Schnurr, John Schulman, Daniel Selsam, Kyla Sheppard, Toki Sherbakov, Jessica Shieh, Sarah Shoker, Pranav Shyam, Szymon Sidor, Eric Sigler, Maddie Simens, Jordan Sitkin, Katarina Slama, Ian Sohl, Benjamin Sokolowsky, Yang Song, Natalie Staudacher, Felipe Petroski Such, Natalie Summers, Ilya Sutskever, Jie Tang, Nikolas Tezak, Madeleine B. Thompson, Phil Tillet, Amin Tootoonchian, Elizabeth Tseng, Preston Tuggle, Nick Turley, Jerry Tworek, Juan Felipe Cerón Uribe, Andrea Vallone, Arun Vijayvergiya, Chelsea Voss, Carroll Wainwright, Justin Jay Wang, Alvin Wang, Ben Wang, Jonathan Ward, Jason Wei, CJ Weinmann, Akila Welihinda, Peter Welinder, Jiayi Weng, Lilian Weng, Matt Wiethoff, Dave Willner, Clemens Winter, Samuel Wolrich, Hannah Wong, Lauren Workman, Sherwin Wu, Jeff Wu, Michael Wu, Kai Xiao, Tao Xu, Sarah Yoo, Kevin Yu, Qiming Yuan, Wojciech Zaremba, Rowan Zellers, Chong Zhang, Marvin Zhang, Shengjia Zhao, Tianhao Zheng, Juntang Zhuang, William Zhuk, and Barret Zoph. Gpt-4 technical report, 2024.

Judea Pearl. Direct and indirect effects. In *Probabilistic and causal inference: the works of Judea Pearl*, pages 373–392. 2022.

Keisuke Sakaguchi, Ronan Le Bras, Chandra Bhagavatula, and Yejin Choi. Winogrande: An adversarial winograd schema challenge at scale. *Communications of the ACM*, 64(9):99–106, 2021.

Alessandro Stolfo, Ben Wu, Wes Gurnee, Yonatan Belinkov, Xingyi Song, Mrinmaya Sachan, and Neel Nanda. Confidence regulation neurons in language models. *arXiv preprint arXiv:2406.16254*, 2024.

Hugo Touvron, Thibaut Lavril, Gautier Izacard, Xavier Martinet, Marie-Anne Lachaux, Timothée Lacroix, Baptiste Rozière, Naman Goyal, Eric Hambro, Faisal Azhar, Aurelien Rodriguez, Armand Joulin, Edouard Grave, and Guillaume Lample. Llama: Open and efficient foundation language models, 2023. URL `https://arxiv.org/abs/2302.13971`.

Ashish Vaswani, Noam Shazeer, Niki Parmar, Jakob Uszkoreit, Llion Jones, Aidan N Gomez, Łukasz Kaiser, and Illia Polosukhin. Attention is all you need. *Advances in neural information processing systems*, 30, 2017.

Jiaxi Wang, Ji Wu, and Lei Huang. Understanding the failure of batch normalization for transformers in nlp. *Advances in Neural Information Processing Systems*, 35:37617–37630, 2022a.

Kevin Wang, Alexandre Variengien, Arthur Conmy, Buck Shlegeris, and Jacob Steinhardt. Interpretability in the wild: a circuit for indirect object identification in gpt-2 small. *arXiv preprint arXiv:2211.00593*, 2022b.

Eric Winsor. Re-examining layernorm. *Alignment Forum*, 2022. URL `https://www.alignmentforum.org/posts/jfG6vdJZCwTQmG7kb/re-examining-layernorm`.

Guangxuan Xiao, Yuandong Tian, Beidi Chen, Song Han, and Mike Lewis. Efficient streaming language models with attention sinks. *Advances in Neural Information Processing Systems*, 37, 2024. arXiv:2309.17453.

Itay Yona, Ilia Shumailov, Jamie Hayes, Federico Barbero, and Yossi Gandelsman. Interpreting the repeated token phenomenon in large language models. *arXiv preprint arXiv:2503.08908*, 2025.

Rowan Zellers, Ari Holtzman, Yonatan Bisk, Ali Farhadi, and Yejin Choi. Hellaswag: Can a machine really finish your sentence? In *Proceedings of the 57th Annual Meeting of the Association for Computational Linguistics*, 2019.

Biao Zhang and Rico Sennrich. Root mean square layer normalization, 2019.

Fred Zhang and Neel Nanda. Towards best practices of activation patching in language models: Metrics and methods. *arXiv preprint arXiv:2309.16042*, 2023.

Jiachen Zhu, Xinlei Chen, Kaiming He, Yann LeCun, and Zhuang Liu. Transformers without normalization, 2025.

Appendix

A Code and Model Availability

The LN removal code is available on: `https://anonymous.4open.science/r/rm-LN-repo/`

Table 2: Hugging Face links for models used and generated in this manuscript. The final links will be shared upon publication due to double-blind review requirements. Furthermore, fine-tuning (FT) steps and GPU hours are shown.

Model	FT Steps	FT GPU Hours	Link
GPT-2 Small original	0	N/A	
GPT-2 Small vanilla	300	1	
GPT-2 Small LN-free	300	1.5	
GPT-2 Medium original	0	N/A	
GPT-2 Medium vanilla	500	2.5	
GPT-2 Medium LN-free	500	3.5	
GPT-2 Large	0	N/A	
GPT-2 Large vanilla	600	6.5	
GPT-2 Large LN-free	600	8	
GPT2 XL original	0	N/A	
GPT2 XL vanilla	800	14	
GPT2 XL LN-free	800	26	

Other Compute Requirements: The evaluation and interpretability experiments require a negligible amount of compute (on the order of a few GPU hours).

B Blockwise LN-Removal Schedules

All schedules use a warmup phase, cosine learning rate decay schedule, and continue fine-tuning for some iterations after LN removal is completed. Recomputation and auxiliary loss are applied to all schedules. The removal steps in the schedule are configured by start, gap and number of layers hyper parameters Tab. 3; See Tab. 4 for how these affect the final schedules.

Hyperparameter	Small	Medium	Large	XL
Original GPT-2 model	gpt2	gpt2-medium	gpt2-large	gpt2-xl
Micro Batch Size	32	22	28	18
Gradient Accumulation Steps	16	23	18	28
Batch Tokens Per Step	524288	518144	516096	516096
Weight Decay	0.01	0.01	0.01	0.01
Learning Rate	0.0006	0.0006	0.0003	0.0001
Min Learning Rate	0.0003	0.0003	0.00004	0.00002
Aux Loss Weight	0.1	0.1	0.03	0.01
Gradient Checkpointing	true	true	false	false
GPU memory	80GB	80GB	180GB	180GB
Number of Layers	12	24	36	48
Warmup Steps	25	10	15	20
Max Steps	300	500	1200	1200
Start LN_{MLP}	20	20	30	50
Start LN_{qk}	44	68	174	242
Start LN_{v}	68	116	318	434
Start LN_{f}	104	188	534	722
Gap LN_{MLP}	2	2	4	4
Gap LN_{qk}	2	2	4	4
Gap LN_{v}	3	3	6	6

Table 3: Comparison of GPT-2 Small, Medium, Large, and XL LN-free Hyperparameters

	Small (12 layers)		Medium (24 layers)		Large (36 layers)		XL (48 layers)	
	Step	Removal	Step	Removal	Step	Removal	Step	Removal
MLP	20	LN^0_{MLP}	20	LN^0_{MLP}	30	LN^0_{MLP}	50	LN^0_{MLP}
	22	LN^1_{MLP}	22	LN^1_{MLP}	34	LN^1_{MLP}	54	LN^1_{MLP}
	...	...	...	...	...	...	...	...
	42	LN^{11}_{MLP}	66	LN^{23}_{MLP}	170	LN^{35}_{MLP}	238	LN^{47}_{MLP}
QK	44	LN^0_{qk}	68	LN^0_{qk}	174	LN^0_{qk}	242	LN^0_{qk}
	46	LN^1_{qk}	70	LN^1_{qk}	178	LN^1_{qk}	246	LN^1_{qk}
	...	...	...	...	...	...	...	...
	66	LN^{11}_{qk}	114	LN^{23}_{qk}	314	LN^{35}_{qk}	430	LN^{47}_{qk}
V	68	LN^0_{v}	116	LN^0_{v}	318	LN^0_{v}	434	LN^0_{v}
	71	LN^1_{v}	119	LN^1_{v}	324	LN^1_{v}	440	LN^1_{v}
	...	...	...	...	...	...	...	...
	101	LN^{11}_{v}	185	LN^{23}_{v}	528	LN^{35}_{v}	716	LN^{47}_{v}
Final	104	LN^f	188	LN^f	534	LN^f	722	LN^f

Table 4: LN removal schedule for GPT-2 Models (Small, Medium, Large, and XL). Values correspond to fine-tuning steps when a particular LN is removed. Gaps between removal events are uniform within each LN group.

B.1 Empirical Guidelines for Hyperparameter Selection

Based on our empirical observations during the development of the LN-removal procedure, we identified several common failure modes and here we provide effective mitigation strategies:

Exploding loss after removal events: If the main loss spikes dramatically shortly after removing a LN module, this typically indicates that the removal schedule is too aggressive. The most effective mitigation is to increase the gaps between removal events within each LN group.

Loss degradation after complete LN removal: When the loss begins to increase after all LN modules have been removed, we found it beneficial to increase the minimum learning rate of the learning rate schedule.

Sudden failures at some fine-tuning step during the query/key path LN removal schedule: In this specific case, we found it beneficial to monitor standard deviation values for drop in replacement, modify the EMA smoothing factor, change the learning rate, and change the auxiliary loss weight.

These strategies proved effective for achieving stable LN removal across all model sizes. Additionally, the auxiliary loss and EMA estimation significantly helped in reducing sensitivity to hyperparameter choices compared to approaches without these components.

C Generalization Beyond GPT-2 Family

To evaluate whether our LN removal methodology extends beyond the GPT-2 model family, we conducted additional experiments using Pythia 70M [Biderman et al., 2023]. We compared two fine-tuning approaches on The Pile dataset: vanilla fine-tuning with LN intact, and our proposed fine-tuning strategy where LN is removed.

The results demonstrate comparable performance degradation to our GPT-2 findings. The vanilla fine-tuned model achieved a cross-entropy loss of 3.80 on the OpenWebText evaluation set, while the LN-free variant achieved a cross-entropy loss of 3.89. This 0.09 increase in loss aligns closely with the performance gap observed in GPT-2 Small (124M parameters), indicating that our methodology exhibits consistent behavior across different transformer architectures. On the HellaSwag benchmark, the original Pythia 70M model scored 0.2679, the vanilla fine-tuned model achieved 0.2667, and the LN-free model obtained 0.2636, showing minimal performance degradation on this alternative evaluation.

These findings provide evidence that our LN removal approach generalizes beyond the specific GPT-2 architecture to other transformer-based language models.

D The Pile-filtered

When evaluating models on the Pile [Gao et al., 2020], we observed unusually high cross-entropy losses for specific tokens. To investigate this, we compared token frequency distributions between 1 million samples from this dataset and OpenWebText [Gokaslan and Cohen, 2019], both pretokenized with GPT-2. We identified tokens that appeared in The Pile but not in OpenWebText, which corresponded to sequences with high cross entropy loss. We filtered out sequences containing any of these tokens, and created a small a 10,000-example filtered subset of The Pile. Upon acceptance, the filtered dataset, along with token metadata and generation scripts, will be made available on the Hugging Face Hub (due to double blind review requirements).

token_id	token	count
197	\t	4,260,185
628	\n\n	1,382,601
1849	\xa0	1,090,135
201	\r	725,891
191	\x03	50,457
200	\x0c	49,412
5624	\xa0	40,045
4603	\xa0\xa0	9,374
205	\x11	5,169
203	\x0f	4,177

Table 5: Top 10 most frequent tokens present in The Pile and missing in OpenWebText.

D.1 GPT-2 XL LN-Free High Loss Samples on The Pile

We reported a very high mean CE loss (130.22) for GPT-2 XL LN-Free on The Pile. However, the median and 99.9 percentile range are very similar to GPT-2 XL original. Three samples are responsible for the high mean CE loss for GPT-2 XL LN-Free on The Pile. We list these samples below. These samples contain a token or token sequence not present in OWT and are listed in Tab. 5. At such tokens, the model has absurdly high CE losses, up to 5 million, i.e., the model is overconfident that the true next token will not be the next. For the three samples, the first token prediction with CE loss larger than 50 are "\x0c", "\t", and "\n" respectively. The last token of the sequence leading up to the token with high errors is "\n" for all three samples, indicating that these specific tokens and token combinations are causing overconfidence in the model. Further inspection reveals that these high CE losses derive from very large negative logits. These outliers occur because, in rare cases involving certain tokens not present in the fine-tuning dataset, the norm of residual stream vectors before unembedding explodes. Interestingly, we observed this phenomenon only in GPT-2 XL.

Sample 1:

```
Sample 2726 out of 10k has tokens with CE loss > 50.

First token with CE loss > 50:200  at position 11.
Decoded:'
'
Decoded (unicode_escape):'\x0c'
Sequence of last 5 Tokens for prediction:220 220 220 1367 198
Decoded:'    11
'
Decoded (unicode_escape):'    11\n'

(Token:Loss)
220:N/A, 220:7.6214733, 220:7.988017, 220:0.7575181, 220:0.21067815, 220:0.11241462, 220:0.0828728, 220:0.07294927,
220:0.06983218, 1367:9.5656, 198:3.8515434, 200:54.273285, 42138:11.611183, 290:5.8352313, 2912:9.315803, 9021:17.121414,
286:5.927439, 8460:9.354071, 642:3.973015, 4310:4.678949, 761:10.288656, 407:0.60814863, 307:0.55970573, 3940:4.7689095,
13:1.346435, 41990:9.208092, 2173:7.9507837, 503:0.88767886, 326:0.47304547, 287:4.0013585, 428:2.462367, 198:7.3526363,
198:0.0011684026, 7442:1.6571776, 11:0.8788041, 262:1.2546973, 20693:6.1989183, 4934:4.3370743, 284:2.2307296, 38040:3.9622679,
10494:0.005666858, 19303:9.20058, 2457:4.18554, 3173:1.1498255, 1682:8.386018, 2058:4.2735405, 407:3.1076946, 422:0.1769652,
262:0.78079456, 198:2.1329598, 198:0.00015055, 36208:13.958086, 4537:12.094295, 16412:8.990057, 475:3.527892, 422:0.22476129,
262:0.55110574, 3893:8.833248, 17541:5.443501, 4347:10.620082, 1799:5.924607, 290:3.480315, 37159:10.124819, 2191:5.4837275,
286:1.5630095, 8235:9.437175, 357:4.602768, 447:6.1605263, 250:5.47846, 39:5.972879, 4061:5.5613327, 3838:6.2311015,
447:4.11596, 251:0.2733165, 828:5.8963223, 198:3.1704738, 198:3.05913, 14876:12.424786, 13:2.642362, 406:8.8554945,
13:4.501826, 1400:6.3063745, 13:2.2849069, 14436:11.087215, 12:3.5680172, 26492:13.83733, 11:2.9488518, 47171:9.930283,
```

8949:10.020365, 11:2.4528143, 15143:9.181636, 11:2.0323732, 22219:9.782476, 11:1.5124732, 9796:9.335302, 5133:8.786331,
13:2.5590122, 27653:13.353212, 11:1.7378397, 27937:10.412004, 11:1.2108434, 15408:11.124487, 11:1.0378554, 1160:8.236352,
6469:10.613097, 357:3.7660804, 22288:7.9838486, 828:5.7518673, 543:3.3631327, 198:4.0904975, 198:0.05241805, 1939:11.162535,
40132:2.9781475, 1115:7.43649, 13788:11.595028, 10411:5.7753525, 8617:7.3080463, 656:7.60578, 13793:10.331831, 22312:10.301449,
11:1.4195569, 262:2.8994842, 18628:10.344179, 20197:7.251051, 6127:7.2656045, 11:2.1663508, 290:2.5125058, 198:4.6340384,
198:2.3188238, 1169:6.9466467, 5094:8.366037, 3893:6.32104, 4809:6.82047, 2191:6.6650662, 25:4.863468, 628:8.807043,
220:8.19655, 220:3.819473, 220:4.2062297, 220:4.961961, 220:4.995181, 220:5.277912, 383:5.82012, 4986:9.652403,
11:2.5059075, 6414:9.438324, 351:3.5732212, 2665:7.6105623, 14436:8.626756, 286:4.936455, 262:2.6958165, 3893:9.572085,
7276:6.6044493, 4347:11.077166, 1799:6.549804, 290:4.471074, 198:3.295391, 220:5.0134106, 220:6.064687, 220:5.9405313,
220:4.124799, 220:3.2302897, 220:1.6753389, 37159:11.453347, 2191:6.410646, 286:3.9341471, 8235:10.6037035, 11:2.1030743,
743:7.7276053, 38040:13.952975, 10494:12220.764, 884:1568.6077, 6647:2484.7053, 355:883.05884, 743:1939.9294, 307:1384.4974,
3306:2680.565, 198:469.1405, 220:1538.7728, 220:1178.9397, 220:1431.203, 220:1082.1162, 220:1259.7878, 220:1304.2883,
393:397.98828, 5035:2698.9102, 284:456.9895, 3283:2395.4785, 503:1655.8503, 262:674.69543, 8617:3220.739, 286:830.44946,
428:1525.5525, 685:797.9059, 3911:4231.721, 4083:2158.9766, 383:999.2892, 4986:2601.727, 743:1726.6406, 198:450.30127,
220:1403.6172, 220:2175.758, 220:2173.087, 220:1988.6704, 220:1560.3451, 220:1146.8448, 38040:4204.649, 10494:8649.862,
597:1345.0178, 19303:3773.4775, 2457:2029.5072, 3173:1839.6007, 355:568.34094, 262:590.8824, 4986:2062.4531, 15947:2279.8892,
389:1038.8564, 5035:2869.369, 284:779.21716, 198:396.0829, 220:881.5056, 220:1608.5259, 220:2106.2659, 220:1546.5009,
220:1546.5249, 220:1340.715, 3283:2450.9758, 503:1587.5262, 428:1318.5421, 685:882.85913, 3911:3507.6172, 4083:2057.4734,
198:216.41724, 198:246.9541, 1959:2581.9805, 471:1004.4808, 13:41.873535, 50:1349.8, 13:150.74365, 34:1408.8376,
13:197.64563, 8460:2291.2534, 15136:1785.7683, 16:2138.023, 66:1901.7491, 11:178.7539, 2608:2297.8555, 471:1437.7157,

...

Decoded:
11

notice and comment procedures of § 553 need not be followed. Plaintiff points out that in this

case, the statutory authority to promulgate interim final rules actually comes not from the

MHPAEA but from the Health Insurance Portability and Accountability Act of 1996 (''HIPAA''),

Pub. L. No. 104-191, §§ 101, 102, 401, 110 Stat. 1936, 1951, 1976, 2082 (1996), which

incorporated three substantially identical provisions into ERISA, the Internal Revenue Code, and

the Public Health Service Act:

> The Secretary, consistent with section 104 of the Health Care Portability and Accountability Act of 1996, may promulgate such regulations as may be necessary or appropriate to carry out the provisions of this [part]. The Secretary may promulgate any interim final rules as the Secretary determines are appropriate to carry out this [part].

29 U.S.C. § 1191c, 26 U.S.C. § 9833 (replacing ''part'' with ''chapter''), and 42 U.S.C. § 300gg-

92 (replacing ''part'' with ''subchapter'').4 Plaintiff argues that Congress only intended to give the

Secretaries authority to promulgate interim final rules relating to HIPAA and not the MHPAEA,

which was passed twelve years later. However, the MHPAEA's substantive provisions are

amendments to the same sections of ERISA, the Internal Revenue Code, and the Public Health

Service Act that are governed by the HIPAA provisions cited above, and the statutory text clearly

gives the Secretaries authority to promulgate interim final rules to carry out these sections.

Therefore, the Court finds that Congress has authorized the Secretaries to ''promulgate any

interim final rules as the[y] determine[] are appropriate to carry out the'' MHPAEA.

Finding that Congress authorized the promulgation of interim final rules does not end the

inquiry. Although the APA recognizes that Congress may modify the notice and comment

4
This regulatory authority covers part 7 of Subtitle B of Title I of ERISA (29 U.S.C. §§ 1181-91c), Chapter 100 of the Internal Revenue Code (26 U.S.C. §§ 9801-33), and Part A of Title XXVII of the Public Health Service Act (42 U.S.C. §§ 300gg to 300gg-92).

12

procedures called for by § 553, it states that a ''[s]ubsequent statute may not be held to supersede

or modify [§ 553] . . . except to the extent that it does so expressly.'' 5 U.S.C. § 559. ''[T]he

import of the § 559 instruction is that Congress's intent to make a substantive change be clear.''

Ass'n of Data Processing Serv. Orgs., Inc. v. Bd. of Governors, 745 F.2d 677, 686 (D.C. Cir.

1986). The statutory provisions authorizing interim final rules in this case do not mention notice

and comment or any other aspect of the APA. In such a case, the D.C. Circuit has defined the

relevant standard as ''whether Congress has established procedures so clearly different from those

required by the APA that it must have intended to displace the norm.'' Asiana Airlines v. FAA,

134 F.3d 393, 397 (D.C. Cir. 1998).

Defendants rely on two cases in which the D.C. Circuit held that the notice and comment

provisions of § 553 were abrogated by specific statutory provisions authorizing interim final

rules. See Asiana Airlines v. Fed. Aviation Admin., 134 F.3d 393 (D.C. Cir. 1998); Methodist

Hosp. of Sacramento v. Shalala, 38 F.3d 1225 (D.C. Cir. 1994). In Methodist Hospital of

Sacramento, the court was faced with

Sample 2:

Sample 7323 out of 10k has tokens with CE loss > 50.
First token with CE loss > 50:197 at position 10.
Decoded:' '
Decoded (unicode_escape):'\t'
Sequence of last 5 Tokens for prediction:257 4731 7177 13 198
Decoded:' a string array.
'
Decoded (unicode_escape):' a string array.\n'
(Token:Loss)
1003:N/A, 1003:11.26658, 9726:11.162002, 46621:13.591053, 355:5.1217504, 257:1.9146276, 4731:7.4259768, 7177:8.642193,
13:1.57043, 198:1.4427543, 197:51.156723, 12235:14.619279, 39:10.696115, 7465:9.209376, 17635:11.363218, 8841:10.934766,
198:3.474833, 92:13.564951, 198:1.2806269, 198:0.0055186776, 1003:3.836342, 968:7.883165, 49:8.290166, 3798:5.798291,
272:7.7695932, 45356:11.567278, 40109:11.504518, 5860:9.337919, 257:1.5190241, 649:1.7121754, 4554:2.7947285, 543:4.841503,
460:2.3216853, 307:0.686766, 973:0.74536353, 284:0.4934966, 2071:5.992473, 257:1.6754444, 581:7.8475504, 5171:6.433069,
198:3.4856787, 1003:13.67105, 19449:8.2021055, 12:3.5855105, 49:5.30799, 5662:5.4760623, 3141:7.5336666, 13:2.6725016,
198:0.8083212, 1003:15.782787, 198:2.8173897, 1003:15.395724, 24550:5.2747335, 25:0.19102867, 770:2.1424239, 318:1.7225417,
257:1.5685425, 275:8.388821, 83:4.2324853, 10210:5.020052, 7552:5.175566, 49702:11.925024, 422:0.8439282, 33084:4.970866,
13:0.68376416, 785:0.20635764, 14:0.37836862, 12501:8.026502, 445:2.2101464, 14:0.4466647, 17896:7.95566, 4372:3.105786,
14:2.777247, 67:4.3537035, 6098:0.37673652, 17752:5.617012, 198:2.2561002, 1003:12.216859, 290:5.0420575, 4433:4.454626,
257:1.9344062, 2639:6.557314, 5459:0.1832912, 4637:3.1329556, 13:1.564306, 198:0.2661691, 20786:21.258528, 968:1.6345162,
49:0.024241818, 3798:2.4097002, 272:3.8780181, 45356:10.635372, 40109:9.851566, 7:3.763564, 9967:6.12138, 39:6.5091047,
7465:0.047564577, 17635:5.3687067, 8841:1.8500897, 8:6.0806694, 1635:5.2731657, 49:4.241615, 3798:2.2475796, 272:1.7413952,
45356:6.1853223, 40109:9.715792, 1391:10.957037, 198:3.2365587, 197:35.354282, 7783:13.6022215, 1222:7.565274, 49:5.145051,
3798:12.716011, 272:9.562733, 45356:12.930087, 40109:13.774559, 90:9.70529, 12235:5.3254843, 39:13.270555, 7465:12.182639,
25:3.5354931, 2512:9.293187, 39:12.1883745, 7465:14.035143, 92:11.704035, 198:3.7612562, 92:9.557363, 198:4.632967,
198:1.6126469, 20786:11.7582035, 2315:11.252395, 3419:599915.1, 1391:128406.42, 198:21275.512, 197:436295.1, 1003:167360.28,
383:44864.34, 9729:140597.66, 287:10736.5625, 428:79266.625, 2393:104939.37, 389:51231.992, 691:73092.914, 24284:177729.25,
416:58283.36, 2639:149387.14, 11603:219064.45, 13:6765.0703, 198:32484.742, 197:443424.3, 33152:201537.97, 19039:195013.5,
471:62431.207, 37:97675.016, 1135:110187.266, 1443:234881.84, 5459:269756.94, 10049:242653.28, 628:112184.06, 197:436574.7,
34320:148946.5, 38804:172249.12, 40109:219531.69, 7203:188346.6, 41299:237815.0, 5344:139417.62, 1600:119173.45, 20789:137373.7,
47649:202613.36, 5344:148038.86, 40109:232167.31, 5769:212062.88, 45991:286692.56, 828:95972.62, 9701:161537.31,
8:45388.77, 198:26669.29, 197:461318.66, 34320:180015.84, 38804:183880.8, 40109:273160.8, 7203:128039.91, 2220:195715.38,
17602:179212.78, 24455:165867.17, 1600:177894.75, 20789:196518.0, 8912:206497.88, 46047:205311.12,
22417:217080.81, 40109:232314.2, 5769:212559.25, 45991:271713.0, 828:92336.35, 9701:131772.14, 8:71338.83, 198:9289.922,
197:479748.06, 34320:161961.17, 38804:183598.38, 40109:324803.62, 7203:168302.4, 1662:152243.08, 1958:311552.6,
27372:174300.81, 1600:175331.19, 20789:198232.06, 3673:121481.22, 1958:134500.3, 45356:281647.62, 40109:218485.22,

...

```
Decoded:
 // Block hashes as a string array.
 BlockHashes []string
}

// NewRescanBlocksCmd returns a new instance which can be used to issue a rescan
// JSON-RPC command.
//
// NOTE: This is a btcd extension ported from github.com/decred/dcrd/dcrjson
// and requires a websocket connection.
func NewRescanBlocksCmd(blockHashes []string) *RescanBlocksCmd {
 return &RescanBlocksCmd{BlockHashes: blockHashes}
}

func init() {
 // The commands in this file are only usable by websockets.
 flags := UFWebsocketOnly

 MustRegisterCmd("authenticate", (*AuthenticateCmd)(nil), flags)
 MustRegisterCmd("loadtxfilter", (*LoadTxFilterCmd)(nil), flags)
 MustRegisterCmd("notifyblocks", (*NotifyBlocksCmd)(nil), flags)
 MustRegisterCmd("notifynewtransactions", (*NotifyNewTransactionsCmd)(nil), flags)
 MustRegisterCmd("notifyreceived", (*NotifyReceivedCmd)(nil), flags)
 MustRegisterCmd("notifyspent", (*NotifySpentCmd)(nil), flags)
 MustRegisterCmd("session", (*SessionCmd)(nil), flags)
 MustRegisterCmd("stopnotifyblocks", (*StopNotifyBlocksCmd)(nil), flags)
 MustRegisterCmd("stopnotifynewtransactions", (*StopNotifyNewTransactionsCmd)(nil), flags)
 MustRegisterCmd("stopnotifyspent", (*StopNotifySpentCmd)(nil), flags)
 MustRegisterCmd("stopnotifyreceived", (*StopNotifyReceivedCmd)(nil), flags)
 MustRegisterCmd("rescan", (*RescanCmd)(nil), flags)
 MustRegisterCmd("rescanblocks", (*RescanBlocksCmd)(nil), flags)
}
```

Faithless Execution: Fighting Presidential Lawlessness

The first few days of rolling out my new book, Faithless Execution, have been exhilarating, with few things more
gratifying and humbling than the wonderful review by one of my very favorites, PJ Media's own Roger Simon.

It has been uplifting to see how many people really are alarmed-rather than indifferent, as I worried-to the problem of rampant
presidential lawlessness. People really do grasp that the separation of powers, which is so threatened by President

Obama’s usurpation of the powers of the states and other federal departments, really is the key to protecting our liberties. Too much accumulation of power in one government official’s hand-particularly, the Framers observed, the joining of the legislative and executive power in a single department or person-is the road to tyranny.

When people grasp that, they similarly grasp that presidential lawlessness is not a conservative versus liberal issue, nor Republican versus Democrat. It is a question of whether we still aspire to be a republic under the rule of law instead of subjects under presidential whim. If they are not knocked down, the precedents that President Obama is setting for imperial executive power will be available for exploitation by every future president, regardless or party or ideological orientation. That ought to frighten all Americans, not just opponents of the current president’s policies.

I make a sustained attempt in the book to explain that impeachment-the ultimate constitutional response to presidential lawlessness-is a political remedy, not a legal one. You can have a thousand impeachable offenses, but if there is not a strong public will that the president be removed, impeachment is a nonstarter. The political case for removal is the one that is uphill. Establishing the legal case for impeachment-i.e., demonstrating that high crimes and misdemeanors have been committed-is the easy part.// The label and actions expect to be in a flex container. Since this component adds another

```
// wrapping layer to the mdc-snackbar__surface, it should also include flex display.
.mat-mdc-simple-snack-bar {
  display: flex;
}
```

"It was like the Alamo at times. Nothing went for us. It feels like we have lost but the final is over two legs and we have to be delighted with the overall scoreline."

Liverpool first-team captain Steven Gerrard and central defender Jamie carragher were quickly in touch after the win and Heighway added: "They have followed us all the way through.

"They texted us before every game and they have texted us again after the win.

"They are steeped in the history of this club and know what it means to win this tournament."

City’s academy chief Jim Cassell

Sample 3:

Sample 9335 out of 10k has tokens with CE loss > 50.
First token with CE loss > 50:198 at position 155.
Decoded:’
’
Decoded (unicode_escape):’\n’
Sequence of last 5 Tokens for prediction:49704 49704 9705 20379 198
Decoded:’//
’
Decoded (unicode_escape):’//\n’
(Token:Loss)
407:N/A, 407:4.6831055, 1624:7.360232, 326:1.4473916, 345:3.3804011, 2630:7.6741157, 262:1.3505429, 2656:4.104636,
3788:4.6768866, 13:1.0597951, 1002:2.57059, 345:0.35921186, 779:3.5662773, 428:2.6555552, 3788:0.4169199, 287:1.3137746,
257:0.32647714, 1720:1.4579158, 11:0.9270898, 281:3.5136762, 48182:1.3712287, 287:0.2596935, 262:0.058141652,
1720:0.16443609, 10314:0.29576224, 561:0.5035581, 307:0.02398988, 16373:0.48682904, 475:0.81268287,
318:0.05656958, 407:0.007545187, 2672:0.050823122, 13:0.0214831, 198:0.7484702, 17:13.849314, 13:0.13205929, 978:7.044759,
4400:2.0608654, 2723:2.2134705, 6300:2.333941, 1276:0.88757795, 307:0.4205811, 30723:1.4280686, 7498:0.11422959,
355:0.0134238945, 884:0.00481102, 11:0.5958381, 290:0.08005254, 1276:0.2439856, 407:0.08167637, 307:0.025275672,
26521:0.17200725, 276:0.0023700502, 355:0.0029704517, 852:0.14899838, 262:0.0020197486, 2656:0.022728885,
3788:0.20550326, 13:0.04337017, 198:0.31131023, 18:6.3787313, 13:0.00059801334, 770:0.9271791, 4003:1.7363278, 743:1.0793377,
407:0.281329, 307:0.013555973, 4615:0.9492111, 393:0.0392538, 14294:0.19510294, 422:0.03199716, 597:0.038671132,
2723:0.24237014, 6082:0.28850555, 13:0.014584245, 198:0.0928015, 16208:7.4476423, 198:0.10754685, 198:0.00033825875,
49704:7.4027767, 49704:0.059470795, 49704:2.1608517, 49704:1.4772909, 49704:1.1133443, 49704:0.9488324,
9705:2.1151383, 20379:1.1406435, 198:0.10158871, 35343:20.283905, 198:0.5157568, 1635:10.543703, 197:30.43997,
4264:13.305223, 1299:0.07563411, 2438:3.0418704, 329:1.6119438, 281:4.073881, 317:5.7669916, 6242:7.9582887, 33:0.08353172,
2927:11.291942, 1304:2.9536972, 13:1.0874708, 198:1.0187862, 1635:12.628989, 197:33.37102, 59:6.926921, 7753:7.370697,
197:33.560585, 197:31.852251, 3185:14.746413, 34:4.736884, 62:2.4475694, 3838:5.085874, 33833:6.238099, 692:5.69899,
1304:0.86001503, 13:0.34363738, 71:1.2452692, 198:0.81940943, 1635:9.853174, 197:32.87166, 59:3.7674747, 9800:6.4635477,
197:33.271984, 197:31.412739, 36910:15.742162, 3813:8.258679, 67:5.3074374, 24086:2.1277742, 198:0.7815698, 1635:3.943909,
197:33.18875, 59:9.100214, 4475:15.064762, 197:33.80469, 197:38.404465, 21339:16.17667, 11:3.2231097, 352:6.5712805,
301:12.503309, 11:3.5788884, 6244:13.497032, 198:4.3184443, 9466:12.119115, 198:4.7258415, 49704:23.561052, 49704:21.665047,
49704:19.027508, 49704:20.011747, 49704:21.655386, 49704:40.67674, 9705:22.09228, 20379:27.61382, 198:8.27015,
198:399.37866, 49704:809.2328, 49704:763.74054, 49704:722.9032, 49704:811.80115, 49704:693.3036, 49704:730.6386, 9705:677.8175,
20379:544.15265, 198:84.33852, 1003:409.64636, 40348:589.6119, 4932:453.42014, 198:66.265816, 2:368.93063, 361:344.89172,
358:423.16663, 891:447.8988, 11593:460.6718, 3185:463.0637, 34:137.90085, 62:323.4264, 3838:367.394, 33833:424.9605,
46:197.75824, 3069:536.48846, 41237:674.64325, 62:188.37312, 39:61808.293, 834:1737813.5, 198:58819.594, 2:501469.34,
13086:476518.62, 11593:430323.34, 3185:436209.5, 34:149311.72, 62:225198.66, 3838:499536.16, 33833:440378.56, 46:344437.5,
3069:506636.12, 41237:671244.25, 62:330165.34, 39:305198.0, 834:412493.72, 628:283896.75, 197:1610916.9, 7249:487438.94,
440:274647.84, 5662:508110.75, 16820:601000.5, 62:200508.23, 17614:568054.25, 317:109115.234, 6242:376880.62, 2749:538623.9,
4891:787976.1, 1058:368174.3, 14701:435548.7, 30562:738873.94, 198:122744.25, 197:1227677.4, 90:353759.03, 198:107419.83,
197:1258664.6, 197:1695466.2, 197:1546377.4, 197:1209663.6, 197:1201286.0, 197:1118433.5, 3838:524715.4, 33833:448043.62,
4891:523260.6, 3419:404699.94, 1058:314273.38, 12301:389488.12,

....

Decoded:
 must not claim that you wrote the original software. If you use this software in a product, an acknowledgment in the product documentation would be appreciated but is not required.
2. Altered source versions must be plainly marked as such, and must not be misrepresented as being the original software.
3. This notice may not be removed or altered from any source distribution.
*/

```
////////////////////////////////////////////////////////////////////////////////////////////////////////////////////////////////
////////////////////////////////////////////////////////////////
/**
 * Contains code for an AABB collider.
 * \file  OPC_AABBCollider.h
```

```
1071    * \author  Pierre Terdiman
1072    * \date  January, 1st, 2002
1073    */
1074   ////////////////////////////////////////////////////////////////////////////////////////////////////////////////////////////////
1075   ////////////////////////////////////////////////////////////////////
1076
1077   ////////////////////////////////////////////////////////////////////////////////////////////////////////////////////////////////
1078   ////////////////////////////////////////////////////////////////////
1079   // Include Guard
1080   #ifndef __OPC_AABBCOLLIDER_H__
1081   #define __OPC_AABBCOLLIDER_H__
1082
1083    struct OPCODE_API AABBCache : VolumeCache
1084    {
1085         AABBCache() : FatCoeff(1.1f)
1086         {
1087          FatBox.mCenter.Zero();
1088          FatBox.mExtents.Zero();
1089         }
1090
1091     // Cached faces signature
1092     CollisionAABB FatBox;  //!< Box used when performing the query resulting in cached faces
1093     // User settings
1094     float   FatCoeff; //!< mRadius2 multiplier used to create a fat sphere
1095    };
1096
1097    class OPCODE_API AABBCollider : public VolumeCollider
1098    {
1099     public:
1100     // Constructor / Destructor
1101              AABBCollider();
1102     virtual        ~AABBCollider();
1103
1104     ////////////////////////////////////////////////////////////////////////////////////////////////////////////////
1105           ////////////////////////////////////////////////////////////////////////////
1106     /**
1107      * Generic collision query for generic OPCODE models. After the call, access the results:
1108      * - with GetContactStatus()
1109      * - with GetNbTouchedPrimitives()
1110      * - with GetTouchedPrimitives()
1111      *
1112      * \param  cache   [in/out] a box cache
1113      * \param  box    [in] collision AABB in world space
1114      * \param  model   [in] Opcode model to collide with
1115      * \return  true if success
1116      * \warning SCALE NOT SUPPORTED. The matrices must contain rotation & translation parts only.
1117      */
1118     ////////////////////////////////////////////////////////////////////////////////////////////////////////////////
1119           ////////////////////////////////////////////////////////////////////////////
1120          bool   Collide(AABBCache& cache, const CollisionAABB& box, const Model& model);
1121     //
1122          bool   Collide(AABBCache& cache, const CollisionAABB& box, const AABBTree* tree);
1123     protected:
1124          CollisionAABB mBox;   //!< Query box in (center, extents) form
1125          Point   mMin;   //!< Query box min point
1126          Point   mMax;   //!< Query box max point
1127     // Leaf description
1128          Point   mLeafVerts[3]; //!< Triangle vertices
1129     // Internal methods
1130          void   _Collide(const AABBCollisionNode* node);
1131          void   _Collide(const AABBNoLeafNode* node);
1132          void   _Collide(const AABBQuantizedNode* node);
1133          void   _Collide(const AABBQuantizedNoLeafNode* node);
1134          void   _Collide(const AABBTreeNode* node);
1135          void   _CollideNoPrimitiveTest(const AABBCollisionNode* node);
1136          void   _CollideNoPrimitiveTest(const AABBNoLeafNode* node
```

E Evaluation on Standard Benchmarks

We additionally evaluated our models on four widely used benchmarks: BoolQ [Clark et al., 2019], HellaSwag [Zellers et al., 2019], PIQA [Bisk et al., 2020], and WinoGrande [Sakaguchi et al., 2021]. These tasks assess general language understanding, commonsense reasoning, and pronoun resolution. Tables 6–9 report normalized accuracy for each model before and after LayerNorm removal. LN-free models maintain performance comparable to their baselines, with only minor variations across tasks.

Task	GPT-2 XL original	GPT-2 XL vanilla FT	GPT-2 XL LN-free FT
BoolQ	61.8	**62.2**	61.9
HellaSwag	**50.9**	49.8	48.8
PIQA	**70.5**	70.5	69.9
WinoGrande	**58.3**	57.5	56.1

Table 6: Accuracy of GPT-2 XL model variants on BoolQ, HellaSwag, PIQA, and WinoGrande.

Task	GPT-2 Large original	GPT-2 Large vanilla FT	GPT-2 Large LN-free FT
BoolQ	60.5	**62.1**	62.0
HellaSwag	**45.4**	43.4	42.8
PIQA	69.2	68.7	**69.3**
WinoGrande	55.3	**56.2**	54.6

Table 7: Accuracy of GPT-2 Large model variants on BoolQ, HellaSwag, PIQA, and WinoGrande.

Task	GPT-2 Medium original	GPT-2 Medium LN-free FT
BoolQ	58.6	**59.9**
HellaSwag	**39.4**	37.4
PIQA	**66.4**	65.6
WinoGrande	**53.1**	51.5

Table 8: Accuracy of GPT-2 Medium model variants on BoolQ, HellaSwag, PIQA, and WinoGrande.

Task	GPT-2 Small original	GPT-2 Small LN-free FT
BoolQ	48.7	**52.0**
HellaSwag	**31.1**	30.2
PIQA	**62.5**	61.4
WinoGrande	**51.6**	50.9

Table 9: Accuracy of GPT-2 Small model variants on BoolQ, HellaSwag, PIQA, and WinoGrande.

Overall, these results show that LN-free models maintain comparable performance on standard benchmarks, supporting their use in interpretability studies.

F Direct Logit Attribution becomes exact

To quantify the discrepancy between Direct Logit Attribution (DLA) and the Direct Effect (DE), we compute the Normalized Mean Absolute Error (NMAE) through a two-stage process. For each attention head h in the model, we calculate:

$$\text{NMAE}_h = \frac{\frac{1}{N}\sum_{i=1}^{N}|DLA_{i,h} - DE_{i,h}|}{\frac{1}{N}\sum_{i=1}^{N}|DE_{i,h}|} \times 100\% \tag{8}$$

where, i indexes individual sequences in The Pile-Filtered dataset, h indexes attention heads, $DLA_{i,h}$ and $DE_{i,h}$ are the corresponding DLA and DE values for sequence i and head h. We then average across all attention heads to obtain the overall NMAE:

$$\text{NMAE} = \frac{1}{H}\sum_{h=1}^{H}\text{NMAE}_h \tag{9}$$

The original model exhibits an NMAE of 49.07% [29.92%, 66.10%] (95% Confidence Interval - CI), indicating that Direct Linear Attribution (DLA) estimates deviate from direct effect measurements by approximately half of the true effect magnitude on average across all attention heads. The vanilla fine-tuned model demonstrates an even larger discrepancy with an NMAE of 57.85% [38.52%, 74.52%]. In contrast, the LN-free fine-tuned model achieves a perfect 0.00% [0.00%, 0.00%] NMAE, empirically confirming that removing the non-linearity introduced by LN eliminates the discrepancy between DLA and direct ablation methods. This result validates that without LN's non-linearity, the two attribution methods are mathematically equivalent, eliminating the need for linearization approximations, which can be significantly inaccurate.

To ensure our overall NMAE metric was not biased by a few significant outliers, we visualized the per-head NMAE values across all attention heads in GPT-2 Small models (Figure 5). In models with LN, the disagreement is widespread across most attention heads rather than driven primarily by a small number of outliers. Later layers showed NMAE values exceeding 100%. In contrast, the LN-free model shows no disagreement between the both methods, with NMAE values of zero across all heads.

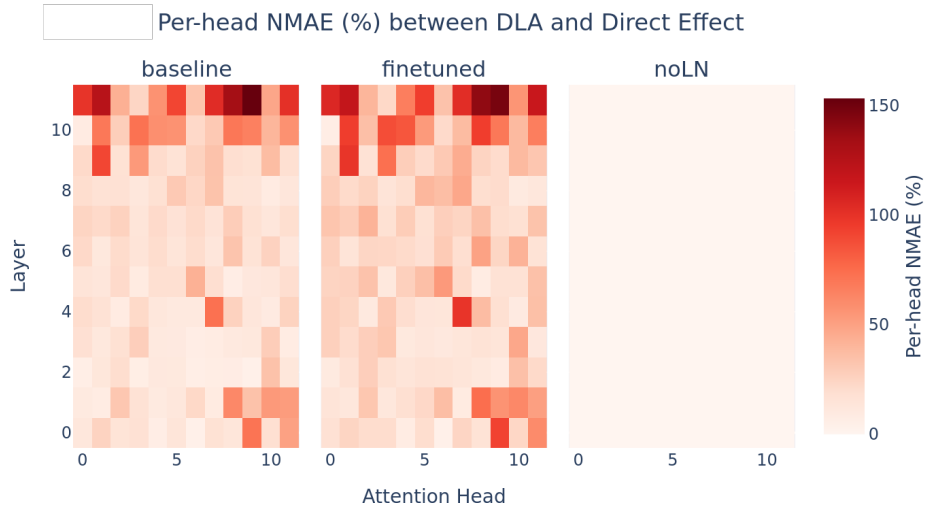

Figure 5: Per-head NMAE (%) between DLA and Direct Effect across all attention heads in GPT-2 Small models: baseline (left), vanilla fine-tuned (middle), and LN-free fine-tuned (right). Significant deviations occur across most attention heads in models with LN. The LN-free model shows no difference across all heads, demonstrating that DLA and DE are equivalent.

G Confidence Neurons

As mentioned in Section 5.4, confidence neurons exhibit two key characteristics: (a) high weight norm, implying importance despite weight decay regularization, and (b) approximately constant contribution to all next token logits, suggesting minimal impact on token prediction. These seemingly contradictory characteristics are reconciled by the final LN, between $\mathbf{w}_{out,i}$ and the unembedding matrix $\mathbf{W}_U$. The effect of confidence neurons on output logits is mediated by this normalization, a mechanism absent in our LN-free models.

These neurons regulate confidence by writing high-norm vectors that project onto an effective nullspace of the unembedding matrix. When these vectors increase the residual stream norm, the final LN scales everything down uniformly, making the output distribution more uniform while preserving token rankings. To identify (b), neurons that preserve token logits ranking, we followed Stolfo et al. [2024] and calculated $\text{LogitVar}(\mathbf{w}_{\text{out},i})$, the variance in the normalized projection of the neuron's weights with each token in the unembedding matrix:

$$\text{LogitVar}(\mathbf{w}_{\text{out},i}) = \text{Var}\left(\frac{\mathbf{W}_{\text{U}}\mathbf{w}_{\text{out},i}}{\|\mathbf{W}_{\text{U}}\|_{dim=1}\|\mathbf{w}_{\text{out},i}\|}\right). \tag{10}$$

Confidence Neurons (CN) maximize the ratio of (a) and (b):

$$\text{CN}(i) = \frac{\|\mathbf{w}_{\text{out},i}\|}{\text{LogitVar}(\mathbf{w}_{\text{out},i})}. \tag{11}$$

Figure 6 summarizes CN identification in both GPT-2 Small and GPT-2 Medium models: the same identical set confidence neurons persist as across all model variants (we chose to highlight the top-7), including LN-free models where their theorized mechanism of action is absent. These neurons maintain their characteristic high weight norm and low logit variance signature despite fine-tuning and even the removal of LN.

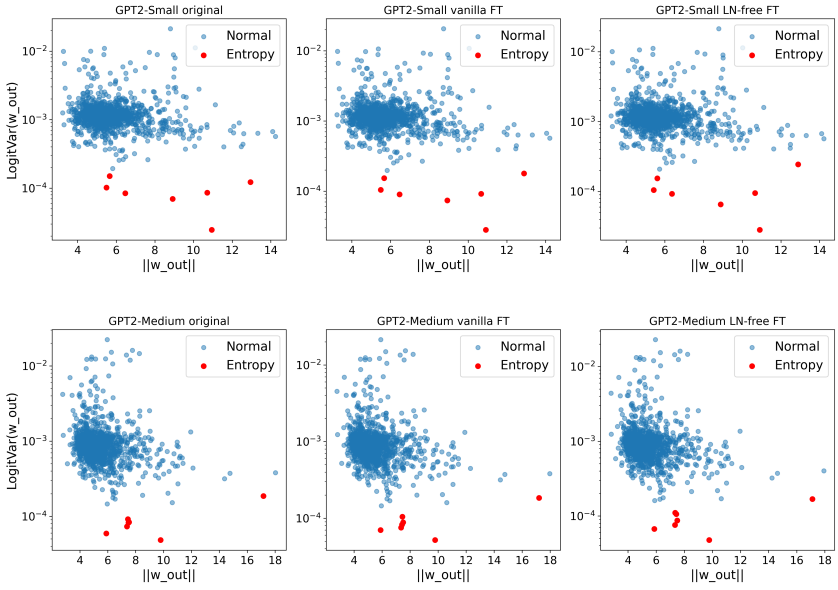

Figure 6: Identification of confidence neurons in GPT-2 Small (top) and GPT-2 Medium (bottom) across different model variants: original pretrained models (left), vanilla fine-tuned models (middle), and LN-free fine-tuned models (right). The same confidence neurons (highlighted in red) persists across all model variants, exhibiting characteristically high weight norms and low logit variance.

Having observed identical confidence neurons across all model variants, we next investigated whether their effective nullspaces were modified by performing Singular Value Decomposition (SVD) on each model's unembedding matrix. Figure 7 shows the normalized singular values (solid lines),

revealing similar nullspace patterns, though fine-tuned variants exhibit a slightly smaller effective nullspace. The cosine similarity between top confidence neurons and singular vectors (dashed lines) demonstrates these neurons predominantly project onto the nullspace in all variants, with some non-negligible overlap in transitional regions where singular values approach zero. This may explain why our vanilla fine-tuned model has less effective confidence regulation when mean ablated. Interestingly, the LN-free model maintains an almost identical nullspace and cosine-similarity pattern to the vanilla fine-tuned model, despite having no ability to affect logit rankings.

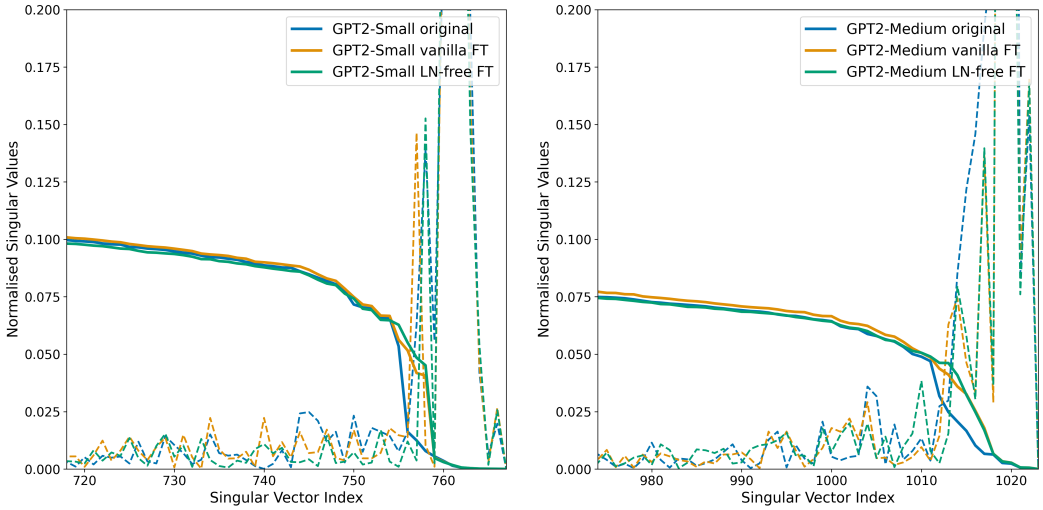

Figure 7: SVD of the unembedding matrix for GPT-2 Small (left) and GPT-2 Medium (right) across model variants. Solid lines show normalized singular values, revealing similar nullspaces across variants, though fine-tuning appears to make the effective nullspace slightly smaller. Dashed lines represent the cosine similarity between the top confidence neuron (584 for Small, 1083 for Medium) and each singular vector. These neurons predominantly interact with the nullspace in all variants, with overlap in regions where singular values approach zero in the fine-tuned models.

To test whether confidence neurons maintain their functional impact across model variants, we performed mean ablation on these neurons (similar to the total effect described in Stolfo et al. [2024]), and measured the resulting change in cross-entropy loss. Figure 8 shows the absolute change in loss when ablating the top-3 confidence neurons in each model. The original GPT-2 Small and GPT-2 Medium models exhibit substantial variation when these neurons are ablated. Without the context-specific LN scaling these neurons provide, the models predicted logit distributions significantly change. The vanilla fine-tuned models show reduced but still notable effects, suggesting these neurons have less effective due to our fine-tuning strategy. This reduced effectiveness may be related to the slightly smaller effective nullspace, though further investigation is needed to confirm this relationship. The LN-free models show almost no variation, implying that these neurons have no effective mechanism to impact final logits despite maintaining their structural characteristics.

To empirically verify that confidence neurons primarily work by modifying the entropy of outputs, we cumulatively ablated the top three confidence neurons in GPT-2 Medium across all variants. Figure 9 illustrates the results. In the original model, ablating all three neurons decreases entropy by over 3% while changing cross-entropy loss by only 0.1%—a 30x difference in magnitude. The vanilla fine-tuned model shows a similar but reduced effect, consistent with our earlier observations of its slightly degraded confidence regulation capability. Again, the LN-free model exhibits no change in either metric. These results directly demonstrate that confidence neurons function by modulating distribution entropy through LN scaling, with minimal impact on which tokens are predicted, allowing them to regulate model uncertainty without changing token rankings. We also investigated whether cumulative confidence neuron ablation of GPT-2 Small vanilla fine-tuned model could yield identical CE loss and entropies to the LN-free model. While the entropies matched (approximately 2.785) when ablating the top-3 neurons, there remained an absolute difference of approximately 0.06 (2%) in CE loss, implying that the general trend of overconfidence in LN-free models arises from more complex mechanisms beyond simply disabled confidence neurons in the final MLP.

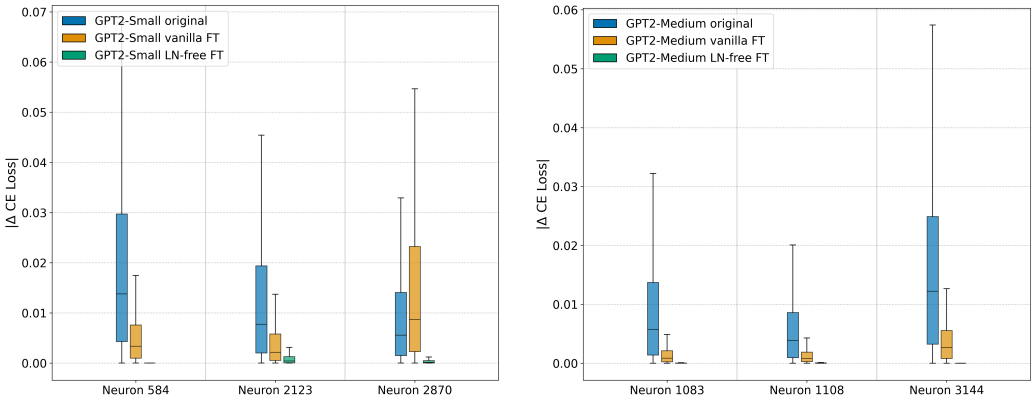

Figure 8: Change in CE loss upon mean ablation of top-3 confidence neurons for GPT-2 Small (left) and GPT-2 Medium (right). The original models (blue) show substantial loss changes when these neurons are ablated, indicating their significant role in confidence regulation. The vanilla fine-tuned models (yellow) exhibit reduced but still notable effects. The LN-free models (green) show almost no change in loss when the same neurons are ablated, confirming that without LN, they lack the mechanism to directly affect output logits.

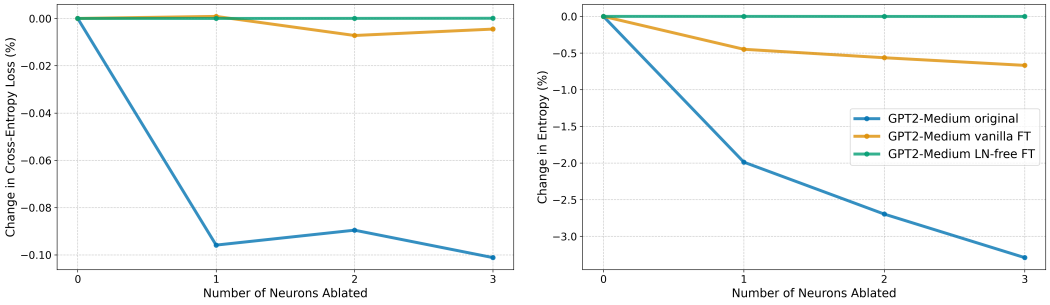

Figure 9: Cumulative effect of ablating the top three confidence neurons in GPT-2 Medium. Left: Relative change in CE loss. Right: Relative change in entropy. The original model (blue) shows a disproportionately large impact on entropy compared to CE loss, demonstrating these neurons primarily regulate distribution confidence rather than token predictions. The vanilla fine-tuned model (yellow) shows reduced effects, while the LN-free model (green) shows no measurable change in either metric.

H Impact Statement

Our work investigates the role of Layer Norm in transformer-based language models, showing that it can be entirely removed from all GPT-2 models with minimal performance loss. This contributes to the broader interpretability agenda by removing nonlinearity and reducing complexity and entanglement. Our results do not move the frontier of model capabilities; thus, we do not expect our work to create novel risks. In contrast, our work may support safer and more transparent model development by making more tractable and accurate mechanistic interpretability techniques. As with other interpretability advances, there remains the possibility that our work could be used to develop more capable AI systems. However, we believe the release of LN-free GPT-2 models will primarily serve researchers working to understand model internals and improve the transparency of current architectures.